On The Dynamics of Multi-Dimensional Detonation

By JIN YAO[1] AND D. SCOTT STEWART[1] †

[1]Department of Theoretical and Applied Mechanics, University of Illinois, Urbana, IL 61801, USA

(28 January 1995)

We outline an asymptotic theory for the dynamics of detonation when the radius of curvature of the detonation shock is large compared to the one-dimensional steady, Chapman-Jouguet (CJ), detonation reaction-zone thickness. The theory includes the limits of near-CJ detonation, and when the normal detonation velocity is significantly below its CJ-value. The curvature of the detonation can also be of either sign corresponding to both diverging and converging geometries. In particular, we derive an intrinsic, partial differential equation (PDE) for the motion of the shock surface, that is hyperbolic in character, and is a relation between the normal detonation shock velocity, shock curvature and the acceleration of the shock along its normal. The derivation includes consideration of additional time-dependence in the slowly-varying reaction-zone than that considered in previous works. A simpler version of the shock evolution equation is derived in the limit of large-activation-energy. Illustrative examples of numerical solutions of intrinsic hyperbolic evolution equations are presented.

---

1. Introduction

Previous work, Stewart & Bdzil (1988), Bdzil & Stewart (1988), has developed an asymptotic theory for weakly-curved, slowly-varying detonation, that propagates near the CJ velocity, D_{CJ}, for the explosive, and has found that the normal detonation shock velocity D_n, is a function of the total shock curvature, κ. We call this relation, the $D_n - \kappa$ - relation, and it is a PDE for the motion of the detonation shock surface. The functional form of the $D_n - \kappa$ - relation follows from an asymptotic argument and is solely determined by the explosive material's equation of state and reaction rate law.

In this paper, we extend the asymptotic analysis by considering additional time-dependence which must be considered when the normal detonation shock velocity deviates significantly from its Chapman-Jouguet (CJ) value. The new description includes both accelerating and decelerating detonations, and the curvature of the detonation can be positive or negative for diverging (convex) or converging (concave) geometries. The only restriction is that the detonation structure has an essential sonic character. This analysis is a significant extension, and replaces the older theory where the detonation normal shock speed is, by assumption, restricted to be near-CJ. In particular, this new theory, re-introduces the time derivatives, which are absent in the older theory. However, an assumption of slow-variation in time, measured on the scale of the particle transit time through the reaction-zone, is still required to carry out a rational set of approximations, where the one-dimensional (1D) steady structure holds to leading order.

† Corresponding Author

The asymptotic technique for analyzing the quasi-steady equations in intrinsic coordinates, used in Stewart & Bdzil (1988) and elaborated on in Klein & Stewart (1993), involves an expansion technique in the $U_n^2 - \lambda$ plane, where U_n is the normal velocity in a shock-attached frame and λ is a progress variable for a forward exothermic reactions. There are essentially two layers, a Main Reaction Layer (MRL), which is a layer that connects the desired (U_n, λ) integral curve to the shock boundary conditions at $\lambda = 0$, and a Transonic Layer (TSL), that connects to the singular point at the intersection of the sonic and thermicity locus, near the end of the reaction layer, with λ near 1. Matching the expansions from either side gives the $D_n - \kappa$ eigenvalue relation, albeit in a somewhat tedious fashion. (When the dimensionless activation-energy is large, then the MRL has a induction-zone (IZ) layer near the shock, and it is appropriate to consider a distinguished limit that reflects how the shape changes of the shock can affect the post-shock temperature. This analysis was recently considered for the steady case, Yao & Stewart (1994).)

The quasi-steady eigenvalue problem, posed in section 4., can be solved numerically, for finite κ, by an iterative shooting technique that starts from the shock and integrates towards the sonic point or vice-versa. Numerically, this procedure is found to be quite robust. For asymptotically small curvature, the numerical shooting technique is equivalent to a method of successive approximation (MSA) technique, which is an alternative to the layer expansion technique. The MSA technique formally integrates a nearly conservative form of the equations in the normal coordinate, from the shock to the generalized CJ-point to obtain integral equations. Integral equations are then used to generate nonsingular asymptotic expansions where the first approximation is a $1D$-steady state. The procedure is general and might be useful for substantial extensions of the related theory; specifically, complex chemistry. It would seem that in most cases that we have tried so far, only one iteration is really all that is required to obtain the essential asymptotic results. Like the numerical approach, the technique is likely to be robust. In what follows, we present the derivation of an unsteady detonation structure that includes acceleration effects using the MSA technique, however we have also carried out the same calculations using the layer expansion procedure. The details of the layer expansions can be found in Yao (1995).

In section 2., we cite the governing equations, explain the intrinsic, shock-attached coordinates used, and present the reduced equations that are analyzed subsequently. Section 2. is read with the help of Appendix I and II, which give details on Betrand-intrinsic coordinates and the reduced governing equations, respectively. Section 3. briefly reviews the one-dimensional steady and quasi-steady states. Section 4. derives the result for quasi-steady, near-CJ detonation and in particular uses the MSA-technique in an integral formulation. Section 5. derives the main asymptotic results for slowly-varying, unsteady, weakly-curved detonation and culminates in the calculation of the $\dot{D}_n - D_n - \kappa$ - relation. Results are displayed for two representative cases, where the equation of state and kinetics parameters correspond to models for condensed-phase and gas-phase detonation. Section 6. separately considers the special case of large activation-energy and derives the $\dot{D}_n - D_n - \kappa$ - relation in the distinguished limit that shock curvature is small on an induction length scale, which is a function of the activation-energy. Section 7. displays some simple numerical solutions that solve for the motion of the detonation shock that obeys representative $\dot{D}_n - D_n - \kappa$ - relations.

2. Governing equations

A standard model of explosive materials is adopted; a compressible Euler fluid, with exothermic reaction. The basic mechanical variables are the velocity, $\vec{u}$, the density ρ and the thermodynamics pressure p. The specific volume is $v = 1/\rho$. Chemistry is modeled in the equation of state by introducing an exothermic chemical reaction, represented by the progress variable, λ. Specification of an equation of state (EOS) of the form $e(p, \rho, \lambda)$, and a rate law, $r(p, \rho, \lambda)$ for λ, is assumed to describe the explosive.

We will further assume the explosive has a polytropic equation of state and an Arrhenius form for the reaction rate,

$$e = \frac{p}{\rho}\frac{1}{\gamma - 1} - Q\lambda, \;\; r(p, \rho, \lambda) = k(1 - \lambda)^{\nu} e^{-E/(p/\rho)}. \tag{2.1}$$

where γ is the polytropic exponent and Q is the heat of combustion, and k, ν, and E are respectively the pre-multiplying reaction rate constant, the depletion factor and the activation-energy. The square of the sound speed is $c^2 = \gamma p/\rho$. This equation of state is the appropriate one for a description of a gaseous explosive. The polytropic equation of state is often used to describe the expansion of explosive products by allowing γ to have artificially higher values than that usually allowed for gases, i.e. $\gamma \sim 2.5 - 3$, with initial densities that are approximately one thousand times larger than those for typical gases. This EOS also has the advantage that a relatively large body of theoretical results exist for it, and which include asymptotic, linear stability and resolved numerical, studies.

The Euler equations are given by

$$\frac{D\rho}{Dt} + \rho\vec{\nabla}\cdot\vec{u} = 0, \;\; \rho\frac{D\vec{u}}{Dt} + \vec{\nabla}p = 0, \;\; \frac{De}{Dt} + p\frac{Dv}{Dt} = 0, \;\; \frac{D\lambda}{Dt} = r(p, \rho, \lambda), \tag{2.2}$$

where $D/Dt \equiv \partial/\partial t + \vec{u}\cdot\vec{\nabla}$. We will assume that the upstream state is quiescent with $\vec{u} = 0$, density ρ_0 and ambient pressure p_0. For convenience, we will assume that the lead detonation shock is sufficiently strong so that the strong-shock approximation holds, (valid when the ratio of the shock pressure to the ambient pressure is very large, i.e. $p_s/p_0 >> 1$.) Also for the strong-shock approximation, the CJ detonation velocity is given by $D_{CJ}^2 = 2(\gamma^2 - 1)Q$.

We now adopt the notation convention where a quantity with a tilde superscript refers to a dimensional quantity and the quantities without a tilde are dimensionless quantities that are scaled with respect to the dimensional unit, unless otherwise specified. In particular, the length, velocity and time-scales are given by $\tilde{\ell}_{rz}, \tilde{D}_{CJ}$ and $\tilde{\ell}_{rz}/\tilde{D}_{CJ}$ respectively. The length $\tilde{\ell}_{rz}$, is taken to be a characteristic 1D, steady reaction-zone length. In section 5., we identify $\tilde{\ell}_{rz}$ as the steady, plane-CJ, half reaction-zone length; the distance from the shock to the point of half-reaction for a steady, plane-CJ detonation. In section 6. we identify $\tilde{\ell}_{rz}$ as an induction-zone length, that is commensurate with the 1/2-reaction length. From (2.1b) we identify the dimensionless rate constant, $k = \tilde{k}\tilde{\ell}_{rz}/\tilde{D}_{CJ}$. The density scale is $\tilde{\rho}_0$ and pressure scale is $\tilde{\rho}_0\tilde{D_{CJ}}^2$. Consequently the sound speed, reaction rate, curvature and heat of combustion appear as $c = \tilde{c}/\tilde{D}_{CJ}$, $r = \tilde{r}\tilde{\ell}_{rz}/\tilde{D}_{CJ}$, $\kappa = \tilde{\kappa}\tilde{\ell}_{rz}, q = \tilde{Q}/\tilde{D}_{CJ}^2 = 1/[2(\gamma^2 - 1)]$.

Later, in the paper, we refer to parameters that use Erpenbeck's scales, Erpenbeck (1964). In his stability studies, Erpenbeck used the density scale, $\tilde{\rho}_0$, the pressure scale, $\tilde{p}_0$, and the velocity scale as the quiescent sound speed, $\tilde{c}_0$. He chose the characteristic length to be the 1/2-reaction length. Erpenbeck's scaled activation energy and the scaled heat release are defined by $E = \tilde{E}/(\tilde{p}_0/\tilde{\rho}_0)$ and $Q = \tilde{Q}/(\tilde{p}_0/\tilde{\rho}_0)$, respectively.

The (dimensionless) normal strong shock relations for an ideal gas moving into an ambient atmosphere, reduce to

$$\rho_s = \frac{\gamma+1}{\gamma-1},\ p_s = D_n^2\frac{2}{\gamma+1},\ U_n \equiv u_n - D_n = -D_n\frac{\gamma-1}{\gamma+1},$$

$$u_t = 0,\ \lambda_s = 0, \tag{2.3}$$

where the $n-$ and $t-$ subscripts respectively refer to the normal component of the shock velocity and the tangential component(s) as defined by the shock normal.

2.1. *Intrinsic geometry and shock-attached coordinates*

In order to make the analysis tractable, the equation of motion must be written in a suitable form. In what follows, we use intrinsic, shock-attached coordinates. The coordinates are specifically based on Betrand curves whose coordinates are instantaneously normal and parallel to the shock surface. Details of the transformation between Cartesian and the Betrand-intrinsic coordinates are described in Appendix I. For brevity, we restrict the presentation that follows to two-dimensions (2D). In the extension to 3D, the curvature that appears in the theory is the sum of the principle curvatures. The shock surface can be represented quite generally in terms of laboratory-fixed coordinates (x, y) by a function $\psi(x, y, t) = 0$. This equation constrains the lab-coordinate position vectors in the surface to $\vec{x} = \vec{x}_s(x, y, t)$. The shock surface can also be represented by a surface parameterization $\vec{x} = \vec{x}_s(\xi, t)$, where ξ measures length along the coordinate lines of the surface. The outward normal (in the direction of the unreacted explosive) and unit tangent vector in the shock surface, (which form a local basis) are given by $\hat{n} = \vec{\nabla}\psi/|\vec{\nabla}\psi|,\ \hat{t} = \partial\vec{x}_s/\partial\xi$. The total shock curvature is given by

$$\kappa(\xi, t) = \vec{\nabla}\cdot\hat{n}. \tag{2.4}$$

Finally, the intrinsic coordinates are related to the laboratory coordinates by the change of variable given by

$$\vec{x} = \vec{x}_s(\xi, t) + n\,\hat{n}(\xi, t), \tag{2.5}$$

where the variables n, ξ are respectively the distance measured in the direction of the normal to the shock wave, and the arclength measured in the shock surface along the principle line(s) of curvature. A more complete description of the Bertrand-intrinsic coordinates is found in Appendix I.

2.2. *Reduced equations in the shock-attached frame*

The governing equations are transformed from a representation in (x,y,t)-coordinates to (n, ξ, t)-coordinates according to coordinate transformation (2.5). The calculations required are straightforward but lengthy. In particular we note, that the normal shock velocity and curvature are only function of ξ and t, i.e. $D_n = D_n(\xi, t)$ and $\kappa = \kappa(\xi, t)$.

Let $U_n = u_n - D_n$, be the relative normal velocity in the shock-attached frame. Appendix II shows that under the assumption that the scaled curvature, $\kappa \to 0$, and that the structure of the flow immediately behind the shock, $(n \le 0, n \sim O(1)\ )$, has weak transverse variations, that the transverse velocity u_ξ can effectively taken to be zero, then the following reduced equations are accurate to $O(\kappa)$. We take these equations to be the starting point for the analysis that follows.

$$\frac{\partial\rho}{\partial t} + \frac{\partial}{\partial n}(\rho U_n) = -\kappa\rho(U_n + D_n), \tag{2.6}$$

$$\frac{\partial U_n}{\partial t} + \dot{D}_n + U_n \frac{\partial U_n}{\partial n} + \frac{1}{\rho}\frac{\partial p}{\partial n} = 0, \tag{2.7}$$

$$\frac{\partial e}{\partial t} + U_n \frac{\partial e}{\partial n} - \frac{p}{\rho^2}\left(\frac{\partial \rho}{\partial t} + U_n \frac{\partial \rho}{\partial n}\right) = 0, \tag{2.8}$$

$$\frac{\partial \lambda}{\partial t} + U \frac{\partial \lambda}{\partial n} = r. \tag{2.9}$$

Next we present the same equations in a quasi-conservative form by placing all the terms where the curvature explicitly appears, and the time-dependent terms on the right-hand side. The right-hand side is associated with small corrections to the essentially, 1D, steady flow. We use the notation $()_{,t} = \partial/\partial t|_{n,\xi}$. We further assume that the time-dependence of the flow is slowly-varying so that $\partial/\partial t \sim o(1)$ as $\kappa \to 0$. As mentioned in Appendix II, for the purpose of further calculation, we replace $\dot{D}_n$ by its approximation, $D_{n,t}$, and write

$$\frac{\partial(\rho U_n)}{\partial n} = -\kappa\rho(U_n + D_n) - \rho_{,t}, \tag{2.10}$$

$$\frac{\partial(\rho U_n^2 + p)}{\partial n} = -\rho_{,t}U_n - \kappa\rho U_n(U_n + D_n) - \rho(U_{n,t} + D_{n,t}), \tag{2.11}$$

$$\begin{aligned}\frac{\partial}{\partial n}\left(\frac{1}{2}U_n^2 + \frac{1}{\gamma-1}c^2 - q\lambda\right) &= -(U_{n,t} + D_{n,t}) \\ &\quad -\frac{1}{U_n}\left(\frac{1}{\gamma-1}\frac{p_{,t}}{\rho} - \frac{\gamma}{\gamma-1}\frac{p}{\rho^2}\rho_{,t} - q\lambda, t\right).\end{aligned} \tag{2.12}$$

The rate equation can be written as

$$\frac{\partial \lambda}{\partial n} - \frac{r}{U_n} = -\frac{\lambda_{,t}}{U_n}. \tag{2.13}$$

The *master equation*

$$(c^2 - U_n^2)\frac{\partial U_n}{\partial n} = qr(\gamma - 1) - \kappa c^2(U_n + D_n) + U_n(U_{n,t} + D_{n,t}) - \frac{p_{,t}}{\rho}, \tag{2.14}$$

is an alternative form of the energy equation, that is used as an auxiliary equation, but is not independent. These equations describe the flow and must satisfy the (strong) shock boundary conditions at $n = 0$.

2.3. *The generalized CJ conditions*

Wood and Kirkwood (1954) first pointed out the essential character of the nonlinear eigenvalue problem that defines the relation between curvature and the normal detonation speed. In particular, they argued that the ordinary differential equations of the quasi-steady, diverging, near-CJ, detonation had to obey both the shock relations and the "generalized CJ conditions", at a sonic point near the end of the reaction-zone. This arises simply from the basic properties of the Euler equations, and the master equation exhibits the special character of the sonic point. Suppose the flow has a sonic point that

$$\eta = c^2 - U_n^2 = 0, \tag{2.15}$$

then equation (2.14) is satisfied at that point, in general, only if, the right hand side, vanishes simultaneously at that point, i.e.

$$qr(\gamma-1)-\kappa c^2(U_n+D_n)+U_n(U_{n,t}+D_{n,t})-\frac{p_{,t}}{\rho}=0. \tag{2.16}$$

The pair of conditions (2.15) and (2.16) taken together are called the "generalized CJ-conditions".

3. One-dimensional steady and quasi-steady states

When the time derivatives and curvature are absent, the conservation laws, given in the preceding section can be integrated to obtain the Rankine-Hugoniot (RH) relations

$$\rho U_n=-D_n, \tag{3.1}$$

$$\rho U_n^2+p={D_n}^2, \tag{3.2}$$

$$\frac{1}{2}U_n^2+\frac{c^2}{\gamma-1}-q\lambda=\frac{1}{2}{D_n}^2. \tag{3.3}$$

The solution of this algebraic system for $U_n, v\equiv 1/\rho$ and p in terms of λ and D_n is

$$U_n=-D_n\frac{\gamma-\ell}{\gamma+1},\quad v=\frac{\gamma-\ell}{\gamma+1},\quad p={D_n}^2\frac{1+\ell}{\gamma+1}, \tag{3.4}$$

where

$$\ell=\sqrt{1-\lambda/{D_n}^2}.$$

Also the sound speed squared and the sonic parameter are given by

$$c^2={D_n}^2\frac{\gamma}{(\gamma+1)^2}(\gamma-\ell)(1+\ell),\quad \eta\equiv c^2-U^2=\frac{{D_n}^2}{(\gamma+1)}\ell(\gamma-\ell). \tag{3.5}$$

The distribution of the reaction is given by the integral

$$n=\int_0^\lambda\frac{U_n}{r}d\bar{\lambda}, \tag{3.6}$$

which can be inverted to obtain $\lambda(n,t)$, where time appears parametrically. Note that sonic parameter η is proportional to ℓ, hence the flow is sonic where $\ell=0$, or whenever $D_n^2=\lambda$.

If the flow is steady and the detonation is overdriven with $D_n>1$, then $\ell>0$ for all $0\le\lambda\le 1$. If $D_n=1$, the CJ-case, then $\ell=0$, when $\lambda=1$. If the wave is underdriven, $D_n<1$, and the sonic point exists for $\lambda=D_n^2<1$ with incomplete combustion at the sonic point. An underdriven 1D detonation cannot be a steady wave throughout all space, however it may still be quasi-steady in some regions. The steady relations formally derived for $D_n<1$ can be used if some portion of the wave, is quasi-steady; for example, between the shock and the sonic point. As we will see this possibility leads to the descriptions of unsteady detonation that travels at sub-CJ velocities that have a simple description in the region between the shock and sonic point. Overdriven detonation may also have a sonic character, so long as D_n is close to one.

4. Quasi-steady, near-CJ, curved detonation

Here we briefly review the essential aspects of the theoretical results for quasi-steady, near-CJ, curved detonation. The emphasis is on illustrating the eigenvalue relation between the normal detonation velocity D_n and the curvature κ. These appear in Stewart & Bdzil (1988), Klein & Stewart (1993), and most recently in Yao & Stewart (1994), for large-activation-energy. Layer asymptotics are used to derive the results, with asymptotic descriptions near the shock, in the main reaction layer and near the sonic point, and the $D_n - \kappa$ - relation is found as a consequence of matching the expansions. However in our review, we present a new technique that obtains the previous formulas, based on approximation to integral equations rather than differential equations.

The mathematical character of the structure problem is described simply in the $U_n^2 - \lambda$ - plane. For the reduced equations, (2.10)-(2.12), set $\partial/\partial t = 0$, and divide the master equation (2.14), by mass equation (2.10) to obtain

$$\frac{dU_n}{d\lambda} = \frac{U_n \Phi}{r\eta} = \frac{U_n[(\gamma-1)qr - \kappa c^2(U_n + D_n)]}{r(c^2 - U_n^2)}, \tag{4.1}$$

subject to the shock boundary condition

$$U_n = -\frac{\gamma-1}{\gamma+1} D_n. \tag{4.2}$$

The reduced Bernoulli's equation (2.12) is integrated to obtain the following expression for c^2,

$$c^2 = \frac{(\gamma-1)}{2}(D_n^2 - U_n^2) + \frac{\lambda}{2(\gamma+1)}. \tag{4.3}$$

The integral curves in the $U_n^2 - \lambda$ - plane are governed by the locus Φ, η and r equal to zero. When the shock is convex, with $\kappa > 0$, there is a saddle point at the intersection of $\eta = c^2 - U_n^2 = 0$ and $\Phi = (\gamma-1)qr - \kappa c^2(U_n + D_n) = 0$. Integral curves leaving the shock point $U_n = -(\gamma-1)/(\gamma+1)D_n$ at $\lambda = 0$, for fixed D_n (say), without a precise value of κ, do not pass through the saddle point and have unphysical structure. Hence there is a unique (eigenvalue) relation between D_n and κ to accommodate passage through the saddle singular point.

Calculation of the $D_n - \kappa$ relation can be carried out in a very simple way as follows. First we find an integrating factor for (4.1) that corresponds to the plane case for $\kappa = 0$. This corresponds to multiplying the above equation (4.1) by the factor $-(\gamma+1)(c^2 - U_n^2)/U_n^3$ and recombining the result to obtain an equation equivalent to (4.1),

$$\frac{d}{d\lambda}\left[\frac{\lambda}{U_n} + \frac{(\gamma^2-1)D_n^2}{U_n} + (\gamma+1)^2 U_n\right] = \kappa \frac{2(\gamma+1)c^2(U_n + D_n)}{rU_n}. \tag{4.4}$$

Note that if the above equation, with $\kappa = 0$ is integrated, with the integration constant evaluated at the shock, one obtains precisely the result that can be obtained from the Rankine-Hugniot relations (3.1) - (3.3), which is quadratic in U_n and expresses conservation of energy throughout the wave structure.

Now integrate (4.4) from the shock to the singular point at $\lambda = \lambda_{CJ}$ to obtain the result at the CJ-point

$$\frac{\lambda_{CJ}}{(U_n)_{CJ}} + \frac{(\gamma^2-1)D_n^2}{(U_n)_{CJ}} + (\gamma+1)^2(U_n)_{CJ} + 2\gamma D_n(\gamma+1) =$$

$$2\kappa(\gamma+1)\int_0^{\lambda_{CJ}} \frac{c^2(U_n+D_n)}{rU_n}d\bar{\lambda}. \tag{4.5}$$

We obtain a correction to the plane value of U_n, (i.e. $\kappa = 0$ value), by an iterative procedure that uses the 1D, quasi-steady CJ solution, (with $U_n = -(\gamma-\ell)/(\gamma+1)$, $c^2 = \gamma(\gamma-\ell)(1+\ell)/(\gamma+1)^2$ and $\ell = \sqrt{1-\lambda}$), as a first approximation in the integral in (4.5), that results in the new approximation

$$\frac{\lambda_{CJ}}{(U_n)_{CJ}} + \frac{(\gamma^2-1)D_n^2}{(U_n)_{CJ}} + (\gamma+1)^2(U_n)_{CJ} + 2\gamma(\gamma+1)D_n =$$

$$-2\kappa(\gamma+1)\gamma I, \tag{4.6}$$

where

$$I \equiv \frac{1}{(\gamma+1)^2}\int_0^{\lambda_{CJ}} \frac{(1+\ell)^2}{r(\ell)}d\bar{\lambda}. \tag{4.7}$$

Enforcing the sonic condition with $c^2 = U_n^2$, in Bernoulli's equation (4.3) obtains the condition

$$(U_n^2)_{CJ} = \frac{(\gamma-1)}{\gamma+1}D_n^2 + \frac{\lambda_{CJ}}{(\gamma+1)^2}. \tag{4.8}$$

Using this result in (4.6) to eliminate $(U_n^2)_{CJ}$, and dropping $O(\kappa^2)$-terms obtains the formula

$$D_n^2 = \lambda_{CJ} - 2\kappa\gamma^2 D_n I. \tag{4.9}$$

The $D_n - \kappa$ relation is found once λ_{CJ} is estimated. This estimate comes from the application of the thermicity condition, $q(r)_{CJ}(\gamma-1) = \kappa(c^2)_{CJ}[(U_n)_{CJ} + D_n]$ which shows that for D_n close to one and κ small,

$$\lambda_{CJ} = 1 - (z^*\kappa)^{1/\nu} + \dots \ . \tag{4.10}$$

Using this result in formula (4.9) obtains

$$D_n = 1 - \kappa\gamma^2 I - \frac{1}{2}(z^*\kappa)^{1/\nu}, \tag{4.11}$$

where $z_* = 2\gamma^2/[(\gamma+1)^2 k_{CJ}]$, and where $k_{CJ} = ke^{\theta/c^2(0)}$, is the leading order value of state-dependent reaction rate pre-multiplier, evaluated at the 1D, CJ-state.

The formula (4.11) agrees precisely with the results found in Stewart & Bdzil (1988)and Klein & Stewart (1993), derived for $0 \le \nu \le 1$. Appendix III has details about the limiting form of the formulas for $\nu < 1$, and includes the logarithmic dependence on κ for $\nu = 1$. Results for the limit of large activation-energy are contained within section 6. Importantly, all the results found in the previous papers are contained in our formula derived here. Note that, only one iteration of the proper integral formulation of the problem posed in the $U_n - \lambda$ plane is needed. This procedure stands in contrast to the more complex expansion techniques of the previous works.

5. Slowly-varying, unsteady, weakly-curved, detonation

Here we add the effect of the normal acceleration of the detonation shock, and calculate its influence on the dynamics of the detonation shock. In particular, we derive an evolution equation for the motion of the shock surface in terms of intrinsic time-derivative of the normal shock velocity, $\dot{D}_n$, the shock normal velocity D_n and the curvature κ; a $\dot{D}_n - D_n - \kappa$-relation. While we are still considering slow-time variation, on the scale of the particle transit time through the reaction- zone of the detonation, we distinguish the results derived here as containing more time-dependence than that considered previously. Hence the description is distinguished as *slowly-varying, unsteady* in contrast to the older theory for which the new time-dependent effects are absent . When it is appropriate to neglect the shock normal acceleration term and set $\dot{D}_n = 0$, the previously derived $D_n - \kappa$ relation is recovered.

We start by integrating equations (2.10) - (2.12) from $n = 0$ to the CJ point, n_{CJ}, and apply the strong shock boundary conditions to obtain integral equations. The first approximation to the solution is the 1D, quasi-steady CJ solution, and it is used to approximate the integral residual terms on the right hand side of the integral equations, which in turn yeild higher-order approximations. For the purpose of generating the corrections, we assume that the detonation velocity and the state has the explicit form

$$D_n = D + \kappa D' \tag{5.1}$$

and

$$U_n = -D\frac{\gamma-\ell}{\gamma+1} + \kappa U', \;\; v = \frac{\gamma-\ell}{\gamma+1} + \kappa v', \;\; p = D^2\frac{1+\ell}{\gamma+1} + \kappa p', \tag{5.2}$$

where $\ell \equiv \sqrt{1-\lambda/D^2}$. To keep notation to a minimum, a * subscript refers to the leading order approximation and a prime superscript is associated with the correction to that approximation, e.g., $U_n = U_*(\ell, D) + \kappa U'$. We represent the leading order approximation to D_n, $(D_n)_*$, by a plain D, where it would appear. All that is assumed for now, in the various expansions (illustrated by the expansion for U_n) is that the correction term $\kappa U' \sim o(U)$ as $\kappa \to 0$. The resulting approximation to the integral equations listed below, have been further simplified by using the first approximation in the integrals on the right hand side of (2.10) - (2.12). Finally we also use the rate equation (2.13) to change the independent variable of integration from n to the progress variable λ to obtain equations for the approximations of ρ, U_n, p and D_n,

$$\rho U_n + D_n(t) = \int_0^n [-\kappa\rho_*(U_* + D) - \rho_{*,t}]d\bar{n} \tag{5.3}$$

$$\rho U_n^2 + p - D_n^2(t) = -\int_0^n [(\rho_* - 1)D_{,t} - \kappa D(U_* + D)]d\bar{n}, \tag{5.4}$$

$$\frac{1}{2}U_n^2 + \frac{c^2}{\gamma-1} - q\lambda - \frac{1}{2}D_n^2(t) = \int_0^n [-\frac{p_{*,t}}{D} - (1 + \frac{D}{U_*})D_{,t}]d\bar{n}\,. \tag{5.5}$$

One calculates the approximate state at the CJ-point, n_{CJ}, where $\lambda = \lambda_{CJ}$, to obtain an approximation to the fluid state there. In particular, it is necessary to calculate the integrals,

$$\int_0^{n_{CJ}} (\rho_{*,t})\, d\bar{n}, \;\; \text{and} \int_0^n \frac{p_{*,t}}{D} d\bar{n}\,.$$

This is done most conveniently using Liebnitz's rule, which we illustrate with the integral over $\rho_{*,t}$. Rewrite the integral as

$$\int_0^{n_{CJ}} (\rho_{*,t})\, d\bar{n} = \frac{\partial}{\partial t}\left(\int_0^{n_{CJ}} \rho_* d\bar{n}\right) - (\rho_*)_{CJ}\frac{\partial n_{CJ}}{\partial t}. \tag{5.6}$$

In turn, $\partial(n_{CJ})/\partial t$ is estimated from differentiating with respect to time, the integral of the distribution of n, i.e.

$$\left[\frac{\partial(n_{CJ})}{\partial t}\right]_{CJ} = \frac{\partial}{\partial t}\left[\int_0^{\lambda_{CJ}} \left(\frac{U_n}{r-\lambda_{,t}}\right) d\bar{\lambda}\right]. \tag{5.7}$$

If we use the rate equation (2.13) to convert the first integral on the right hand side of (5.6), we combine the result to get

$$\int_0^{n_{CJ}} (\rho_{*,t})\, d\bar{n} = \frac{\partial}{\partial t}\left[\int_0^{\lambda_{CJ}} \frac{\rho_* - (\rho_*)_{CJ}}{r-\lambda_{,t}} U_n d\bar{\lambda}\right]. \tag{5.8}$$

Finally, if we use the expressions for ρ_* and U_*, (which contain implicit time dependence through D), and neglect $\lambda_{,t}$, then one finally obtains

$$\int_0^{n_{CJ}} \rho_{*,t} d\bar{n} = \frac{\partial}{\partial D}\left(D\int_0^{\lambda_{CJ}} \frac{\ell}{r} d\lambda\right) D_{,t}. \tag{5.9}$$

By evaluating (5.3) - (5.5) at the CJ-state we obtain a set of Rankine-Hugoniot-like conditions that determine approximations to the CJ-state,

$$(\rho U_n)_{CJ} = -D_n + \kappa I_1 D^2 + J_1 D_{,t}, \tag{5.10}$$

$$(\rho U_n^2)_{CJ} + p_{CJ} = {D_n}^2 - \kappa I_2 D^3 + I_1 D D_{,t}, \tag{5.11}$$

$$\frac{1}{2}(U_n^2)_{CJ} + \frac{c_{CJ}^2}{\gamma-1} - q\lambda_{CJ} = \frac{{D_n}^2}{2} - (I_1+J_2)DD_{,t}, \tag{5.12}$$

where the reaction rate integrals I_1, I_2, J_1, J_2 are given by

$$I_1 = \frac{1}{(\gamma+1)}\int_0^{\lambda_{CJ}} \frac{(1+\ell)}{r} d\lambda, \quad I_2 = \frac{1}{(\gamma+1)^2}\int_0^{\lambda_{CJ}} [\frac{(\gamma-\ell)(1+\ell)}{r}] d\lambda,$$

$$I_3 = \frac{1}{(\gamma+1)^2}\int_0^{\lambda_{CJ}} \frac{\ell(\gamma-\ell)}{r} d\lambda, \quad I_4 = \int_0^{\lambda_{CJ}} \frac{\ell}{r} d\lambda,$$

$$J_1 = \frac{1}{\gamma}\frac{d(DI_4)}{dD}, \quad J_2 = -\frac{1}{D^2}\frac{d(D^3 I_3)}{dD}. \tag{5.13}$$

The formal algebraic solution of equations (5.10) - (5.12) subject to the sonic constraint that $c^2 = U_n^2$, in fact determines the state $\rho_{CJ}, (U_n)_{CJ}, p_{CJ}$ and a condition on the speed D_n, in the same way as is obtained for the simplest case of a steady, plane, CJ wave. For our present purpose the algebra for the states, is solved simply in a few steps. Step one uses the mass equation (5.10) to replace ρ in favor of U_n. Step two divides equation (5.11) by ρ, uses the replacement of ρ in terms of U_n from the previous step, and replaces

p/ρ by c^2/γ. Now the sonic condition $c^2 = U_n^2$ can be used to obtain an equation for U_n alone; which is quadratic, but has the common factor U_n. The relevant root is the other factor which obtains the solution for U_n

$$U_n = -\frac{\gamma}{\gamma+1}\frac{[D_n^2 - \kappa I_2 D^3 + I_1 D D_{,t}]}{[D_n - \kappa I_1 D^2 - J_1 D_{,t}]}. \tag{5.14}$$

An important consequence of the factorization (from the application of the sonic condition) is that the CJ state is linear in the perturbation to the leading order state. The result for U_n, and the sonic condition $c^2 = U_n^2$ can then be used in the remaining equation (5.12) to obtain condition on D_n, which in fact is a condition on $D_{,t}, D_n, \kappa$ and λ_{CJ},

$$D_n^2 - \lambda_{CJ} + \gamma^2 \left\{ \frac{[D_n^2 - \kappa I_2 D^3 + I_1 D D_{,t}]^2}{[D_n - \kappa I_1 D^2 - J_1 D_{,t}]^2} - D_n^2 \right\} + 2(\gamma^2 - 1)(I_1 + J_1) D D_{,t} = 0. \tag{5.15}$$

One can write the formal expressions for p_{CJ} and ρ_{CJ} by back substitution.

The algebratic solutions to this point are formal and are further reduced by only retaining the first corrections in the curvature, κ and the unsteadiness represented by $D_{,t}$. Thus we obtain the reduced expression for the states at the CJ-point

$$v_{CJ} = \frac{\gamma}{\gamma+1} + \frac{\gamma}{\gamma+1}\left[(2I_1 - I_2)D + (I_1 + 2J_1)\frac{D_{,t}}{D}\right], \tag{5.16}$$

$$(U_n)_{CJ} = -\frac{\gamma}{\gamma+1}D - \frac{\gamma}{\gamma+1}\left[\kappa D' + \kappa(I_1 - I_2)D^2 + (I_1 + J_1)D_{,t}\right], \tag{5.17}$$

$$p_{CJ} = \frac{D^2}{\gamma+1} + \frac{D}{\gamma+1}\left[\kappa(2D' - I_2 D^2) + I_1 D_{,t}\right], \tag{5.18}$$

$$(c^2)_{CJ} = \frac{\gamma^2 D^2}{(\gamma+1)^2} + 2\frac{D\gamma^2}{(\gamma+1)^2}\left[\kappa(D' + (I_1 - I_2)D^2) + (I_1 + J_1)D_{,t}\right], \tag{5.19}$$

and a reduced $(D_{,t} - D_n - \kappa - \lambda_{CJ})$-relation,

$$D_n^2 - \lambda_{CJ} + 2\kappa\gamma^2(I_1 - I_2)D^3 + 2DD_{,t}[(\gamma^2 - 1)(I_1 + J_2) + \gamma^2(I_1 + J_1)] = 0. \tag{5.20}$$

In most respects, equation (5.20) is the key result and holds generally for slowly-varying, weakly-curved detonation structure that has a sonic character. The result is not restricted to D_n close to one, and D_n may differ from its CJ-value (one), by an $O(1)$ amount. Also when $D_{,t} = 0$, $D = 1$, and $\lambda_{CJ} \sim 1$, one recovers the $D_n - \kappa$ formulas discussed in the previous section. Also, D_n can be greater than one provided that $D_n \sim 1$, and the formula (5.20) still applies. This corresponds to a slightly overdriven detonation, and section 6. discusses this case in the context of large-activation-energy. While the above formula is quite revealing and contains much of the information needed to write down the evolution equation, the condition imposed by the thermicity condition must be considered, and that is discussed next.

5.1. *The thermicity condition*

If D_n is appreciable different and below one (i.e. to sub-CJ), the balance in the thermicity condition (2.16) at the generalized CJ-point, is between the reaction and time-dependence, (unlike the near-CJ case where it is between curvature and reaction). Recall

that the flow approaches sonic when $\ell = \sqrt{1-\lambda/D^2} \to 0$. Thus $\ell = 0$ corresponds to $\lambda_{CJ} = D^2$ to leading order; however a finer estimate is required in order to obtain closure. The leading order result, leads to an important conclusion. If $D < 1$, then $\lambda_{CJ} < 1$, thus the reaction rate at the sonic point $(r)_{CJ}$, is necessarily $O(1)$, and cannot be balanced by the small curvature term $\kappa c^2(U_n + D_n)$, found in the thermicity condition (2.16). Thus the reaction must be balanced by local unsteadiness, which can be induced by the sonic character of the flow.

For the purpose of analyzing the state in the thermicity condition we write

$$D_n = D + \kappa D' + \ldots, \quad \lambda_{CJ} = D^2 - \lambda' + \ldots, \tag{5.21}$$

where the order of $\lambda' \sim O((D_{,t})^2)$, and is to be confirmed by the analysis. Thus a finer estimate for ℓ near the sonic point is $\ell = \sqrt{\lambda'/D^2}$. The balance of reaction and unsteadiness is illustrated in the derivative $\ell_{,t}$. From the definition of ℓ one finds

$$\ell_{,t} = \frac{1}{\ell D^2}\left(-\frac{1}{2}\lambda_{,t} + \frac{\lambda}{D}D_{,t}\right). \tag{5.22}$$

This formula shows that $\ell_{,t}$ can be $O(1)$ if the flow is quasi-steady, and the flow state is close to sonic, i.e. $\ell_{,t}$ can be calculated as the ratio of two small terms. Since $\ell \sim \sqrt{\lambda'}$ near the sonic-point, we use the definition of $\ell_{,t}$ to obtain an independent formula that can be used to estimate λ',

$$\lambda' = D^2\left[\frac{1}{(\ell_{,t})_{CJ}D^2}\left(-\frac{(\lambda_{,t})_{CJ}}{2} + DD_{,t}\right)\right]^2 \geq 0. \tag{5.23}$$

This formula suggests that when $D < 1$ and $(\ell_{,t})_{CJ} \sim O(1)$, that $\lambda' \sim O[(\lambda_{,t})^2_{CJ}, (D_{,t})^2]$, and can be neglected if the time-variation is sufficiently slow, if $\partial/\partial t \sim O(\kappa)$ (say). When $D \to 1$, λ' can still be small, consistent with $\lambda_{CJ} \to 1$, provided that $(\ell_{,t})_{CJ} \to 0$. This last property is shown from the leading order thermicity condition, expressed at the generalized CJ-point, which is a balance of reaction and time-dependence, and gives the leading order condition,

$$q(\gamma-1)r_{CJ} = 2D^2\frac{\gamma}{(\gamma+1)^2}(\ell_{,t})_{CJ}. \tag{5.24}$$

At the next order of approximation, the thermicity condition (2.16) contains the unsteady terms $U_{,t}$ and $p_{,t}$ which are found approximately by differentiating the respective leading order approximation to U and p, to obtain

$$(U_{,t})_{CJ} = -\frac{\gamma}{\gamma+1}D_{,t} + \frac{D}{\gamma+1}(\ell_{,t})_{CJ} + \ldots,$$

$$(P_{,t})_{CJ} = \frac{2D}{\gamma+1}D_{,t} + \frac{D^2}{\gamma+1}(\ell_{,t})_{CJ} + \ldots \quad . \tag{5.25}$$

For the present purpose, we assume that the reaction rate can be expressed as depletion factor times a state-dependent rate constant of the general form, $r = r(\lambda, c^2)$, and expand appropriately. To simplify notation in what follows, the subscript CJ or a plain variable, without a sub- or super- script, will identify the leading order, or leading order CJ-state, and a prime super-script will be used to define the correction to the state. Expansion of the thermicity condition (2.16) in a straightforward manner obtains the perturbation condition

$$q(\gamma-1)[-(r_{,\lambda})_{CJ}\lambda' + (r_{,c^2})_{CJ}(c^2)'] - \kappa\,(c^2)_{CJ}\frac{D}{\gamma+1} - 3\frac{\gamma}{(\gamma+1)^2}DD_{,t}$$

$$+\frac{D}{\gamma+1}(\ell_{,t})_{CJ}\,[\kappa U' - D\kappa v'] = 0, \tag{5.26}$$

where

$$(r_{,\lambda})_{CJ} = -\nu(r)_{CJ}/(1-D^2), \quad (r_{,c^2})_{CJ} = \theta(r)_{CJ}/[\,(c^4)_{CJ}]. \tag{5.27}$$

The c^2-perturbation is known from the U^2-perturbation, $(c^2)' = 2U_{CJ}\kappa U'$; the expression for $(\ell_{,t})_{CJ}$ is calculated from (5.24), and the U- and v-perturbations at the CJ-state were previously determined from the RH algebra, (5.17) and (5.16) are listed here for convenience: $\kappa U' = -[\gamma/(\gamma+1)]\,[\kappa D' + \kappa(I_1-I_2)D^2 + (I_1+J_1)D_{,t})]$ and $\kappa v' = [\gamma/(\gamma+1)]\,[(2I_1-I_2)D + (I_1+2J_1)D_{,t}/D]$.

The correction to the thermicity condition, (5.26) is a linear relation in the quantities $\lambda', \kappa D', D_{,t}$ and κ. A second linear relation follows simply from the sonic condition (5.20). By substituting the expansions for D_n and λ_{CJ} into (5.20), with the limit of integration in the integrals taken to be $\lambda_{CJ} = D^2$, one obtains

$$2DD'\kappa + \lambda' + 2\kappa\gamma^2(I_1-I_2)D^3 + 2DD_{,t}[(\gamma^2-1)(I_1+J_2) + \gamma^2(I_1+J_1)] = 0. \tag{5.28}$$

The solution of (5.26) and (5.28) for λ' and $\kappa D'$, obtains

$$\lambda' = \frac{Bb_1 - 2Db_2}{B + 2D(r_{,\lambda})_{CJ}}, \quad \kappa D' = \frac{(r_{,\lambda})_{CJ}b_1 + b_2}{B + 2D(r_{,\lambda})_{CJ}}, \tag{5.29}$$

where

$$B = -(r)_{CJ}\left[\frac{1}{2D} - 2D\frac{\gamma^2}{(\gamma+1)^2}\frac{\theta}{(c^4)_{CJ}}\right], \tag{5.30}$$

where b_1 and b_2 are

$$b_1 = b_{11}\kappa + b_{12}\dot{D}_n, \quad b_2 = b_{21}\kappa + b_{22}\dot{D}_n, \tag{5.31}$$

with the coefficients

$$b_{11} = -2\gamma^2(I_1-I_2)D^3, \tag{5.32}$$

$$b_{12} = -2D[\gamma^2(I_1+J_1) + (\gamma^2-1)(I_1+J_2)], \tag{5.33}$$

$$b_{21} = 2D^3\frac{\gamma^2}{(\gamma+1)^2} + r_{CJ}D[\frac{1}{2}(3I_1-2I_2) - 2D^2\frac{\gamma^2}{(\gamma+1)^2}(I_1-I_2)\frac{\theta}{c_{CJ}^4}], \tag{5.34}$$

$$b_{22} = 6D\frac{\gamma}{\gamma+1} + \frac{r_{CJ}}{D}[\frac{1}{2}(2I_1+3J_1) - 2D^2\frac{\gamma^2}{(\gamma+1)^2}(I_1+J_1)\frac{\theta}{c_{CJ}^4}]. \tag{5.35}$$

An independent equation for λ' is obtained from (5.23), and is needed in order to calculate a uniform approximation to the $\dot{D}_n - D_n - \kappa$-relation, for D close to and below one. This is reflected in the fact that while λ' is generally small and can be neglected for

$D < 1$; it strictly cannot be neglected in the limit $D \to 1$. Note that in (5.23), $(\lambda_{,t})_{CJ}$ appears, and can be estimated from the rate equation as

$$\left(\frac{\partial \lambda}{\partial t}\right)_{CJ} = -\frac{(r)_{CJ}}{U_{CJ}} J D_{,t}, \text{ where } J = \int_0^{D^2} \frac{\partial (U/r)}{\partial D} d\lambda. \tag{5.36}$$

Using the above estimate and the expression for $(\ell_{,t})_{CJ}$ from (5.24) in (5.23) obtains an estimate for λ' in terms of D and $D_{,t}$

$$\lambda' = \frac{G(D)}{(r_{CJ})^2}(D_{,t})^2 \text{ where } G(D) = \left[\frac{2\gamma}{(\gamma+1)}\left(2 + \frac{r_{CJ}}{U_{CJ}}\frac{J}{D}\right)\right]^2. \tag{5.37}$$

Finally, we use the above result, (5.37) and the definition of $D_n = D + \kappa D'$, in (5.29 a, b) to rewrite them as two relations between $D_{,t}, D_n, \kappa$ (in terms of the parameter D)

$$C_1 D_{,t}^2 + C_2 D_{,t} + C_3 \kappa = 0, \tag{5.38}$$

$$D_n = D + \frac{[b_{21} + (r_{,\lambda})_{CJ} b_{11}]\kappa + [b_{22} + (r_{,\lambda})_{CJ} b_{21}] D_{,t}}{B + 2D(r_{,\lambda})_{CJ}}, \tag{5.39}$$

where

$$\begin{aligned} C_1(D) &= \frac{G}{r_{CJ}^2}(B + 2D(r_{,\lambda})_{CJ}), \\ C_2(D) &= -Bb_{12} + 2Db_{22}, \\ C_3(D) &= 2Db_{21} - Bb_{11}. \end{aligned} \tag{5.40}$$

5.2. *Intrinsic evolution equation*

As the $D_n - \kappa$-relation in the original theory was reduced to finding a curve for the response of the detonation in a $D_n - \kappa$ plane, it is useful to regard the $\dot{D}_n - D_n - \kappa$-relation as a surface in a $\dot{D}_n - D_n - \kappa$ - space. The surface is determined by eliminating the parameter D from (5.38) and (5.39) in favor of $D_{,t}, D_n$ and κ. Also we note that to the order that is calculated here, the derivative $D_{,t} \equiv \partial D/\partial t|_{(\xi,n)}$ represents the intrinsic derivative $\dot{D}_n$, hence we replace $D_{,t}$ by $\dot{D}_n$.

Note that by elimination of D from (5.38), (5.39), for $D \leq 1$, one generates a $\dot{D}_n - D_n - \kappa$-relation, that uniformly allows for values of D_n below one and D_n close to one. D_n may be in the range from less than one, to slightly greater than one. D_n is not allowed to be greater than one by an $O(1)$ amount. The restriction that maximum of D_n can only be slightly greater than one, follows from the loss of the sonic character of the flow if the wave is strongly overdriven. For an overdriven flow $D > 1$, the flow behind the complete reaction point is subsonic, and in the most general case, one must solve the Euler equations in combination with the conditions presented by the completely reacted reaction-zone. Because of the appearance of the rate integrals I_1, I_2, J_1, J_2, etc., the general case for all $D \leq 1$, is somewhat complicated and requires numerical evaluation to display the results. Indeed the composite description of the surface has two distinct branches, as we will illustrate in section 5.2.2., for $D < 1$ and section 5.2.3. for $D \sim 1$. But the formula presented here can be used to generate the $\dot{D}_n - D_n - \kappa$-relation as a surface, for finite but small κ and $\dot{D}_n$.

5.2.1. *Hyperbolicity and local stability*

The branches of the $\dot{D}_n - D_n - \kappa$-relation must be checked to ensure that it corresponds to a hyperbolic PDE. This additional classification criterion derives from a frozen-coefficient analysis of the intrinsic PDE, and can be summarized as follows. Suppose that a differentiable relation exists of the form, $F(\dot{D}_n, D_n, \kappa) = 0$, and that we are interested in the character of the evolution of the shock surface in a neighborhood of the starred values, $(\dot{D}_n)^*, (D_n)^*, (\kappa)^*$. Only for the purpose of analyzing the local dynamics at small-times, we consider a local Cartesian coordinate system along the normal, and tangent to the normal. Let x be in the tangential direction, and let ϕ be a displacement along the shock along the normal. Then we further assume that the shock is now described by the expansions

$$\dot{D}_n = (\dot{D}_n)^* + \phi_{,tt} + \ldots, \quad D_n = (D_n)^* + \phi_{,t} + \ldots, \quad \kappa = (\kappa)^* - \phi_{,xx} + \ldots, \quad . \tag{5.41}$$

Insertion of the expansion (5.41) into , $F(\dot{D}_n, D_n, \kappa) = 0$, and the neglect of higher order terms leads to the linear PDE,

$$-\left(\frac{\partial \kappa}{\partial \dot{D}_n}\right)^*_{D_n} \phi_{,tt} - \left(\frac{\partial \kappa}{\partial D_n}\right)^*_{\dot{D}_n} \phi_{,t} + \phi_{,xx} = 0. \tag{5.42}$$

where we used the identities

$$(\partial F/\partial \dot{D}_n)^*/(\partial F/\partial \kappa)^* = -(\partial \kappa/\partial \dot{D}_n)^*, \quad (\partial F/\partial D_n)^*/(\partial F/\partial \kappa)^* = -(\partial \kappa/\partial D_n)^*.$$

The condition for hyperbolicity that follows is simply that at each point on the surface that

$$\left(\frac{\partial \kappa}{\partial \dot{D}_n}\right)^*_{D_n} < 0. \tag{5.43}$$

The local stability of spatial disturbances depends on the sign of the term $(\partial \kappa/\partial D_n)^*_{\dot{D}_n}$. This follows from the dispersion relation, which is found by substituting $\phi = exp[\lambda t + i\, kx]$, into (5.42) and deriving the quadratic for $\lambda(k)$. One obtains the conclusion

$$\left(\frac{\partial D_n}{\partial \kappa}\right)_{\dot{D}_n} \begin{cases} < & 0 \text{ stable} \\ > & 0 \text{ unstable} \end{cases} . \tag{5.44}$$

In previous works, where $\dot{D}_n$ is absent, the stability of the corresponding $D_n - \kappa$-relation obeys that of the heat equation and the condition shown in (5.44) applies. In particular the under-side of the $D_n - \kappa$, curve, where $\partial D_n/\partial \kappa > 0$, incorrectly was thought to be necessarily unphysical, since it corresponded to instability. In general, the response is only locally unstable, and nonlinear evolution consistent with the underlying hyperbolic dynamics, is possible. In particular, for sub-CJ, detonation in the presence of positive curvature, shock acceleration is possible, which allows for the nonlinear growth and acceleration of convex portions of the shock. This is likely to be a key ingredient in the growth and propagation of detonation cells.

5.2.2. *Sub-CJ detonation:* $D < 1$

When D_n is significantly below one, $(D < 1)$, then $\lambda' \sim O[(D_{,t})^2]$ and we may neglect it. The balance in the thermicity condition is only between reaction and time-dependence. D_n is accurately described to leading order by D. Then equation (5.29 a) shows with

(λ' set equal to zero) that the surface is represented by $\beta b_1 = 2D_n b_2$ (with D_n replacing D). This equation can be re-expressed as

$$\dot{D}_n + A(D_n)\kappa = 0, \tag{5.45}$$

where

$$A(D_n) = C_3(D_n)/C_2(D_n) \tag{5.46}$$

Note that $A(D_n) > 0$, hence by classification theory, the intrinsic PDE, is guaranteed to be hyperbolic.

Importantly, as $D \to 1$, for $D < 1$, the limit of this branch of the surface is tangent to a plane, that is only a linear $\dot{D}_n - \kappa$ relation. Note that as $D \to 1$, $\beta \to 0$ and the evolution equation reduces to simply, $b_2 = 0$ (with $D = 1$) or

$$\dot{D}_n + \frac{\gamma}{3(\gamma+1)}\kappa = 0. \tag{5.47}$$

Notice that $\dot{D}_n = 0$ corresponds to $\kappa = 0$ for all D_n.

5.2.3. *Near-CJ detonation:* $D \sim 1$

The other limiting branch of the surface is found by starting with the limit $D \to 1$. The balance in the thermicity condition can be between reaction and time-dependence and curvature effects. As a result of the influence of curvature, the surface can be dependent on the depletion factor ν.

To illustrate this branch, note that as $D \to 1$ that $(r_{,\lambda})_{CJ} \to \infty$. Then (5.29 b) reduces to the limit $\kappa D' = b_1/2$. Then if we replace $\kappa D' = D_n - 1$, we obtain a second branch of the surface that is only valid near $D, D_n \sim 1$;

$$D_n = 1 - \kappa\gamma^2(I_1 - I_2) - \dot{D}_n[(\gamma^2 - 1)(I_1 + J_2) + \gamma^2(I_1 + J_1)]. \tag{5.48}$$

In the case when the integrals I_1, etc. are constants, (which is the case for finite-activation-energy), then the above equation is also a plane in the $\dot{D}_n - D_n - \kappa$ - plane. The $\dot{D}_n - D_n - \kappa$-plane found in this limit is also shown to be a hyperbolic PDE, however with a different transverse wave speed than for the branch $D < 1$. Also, classification theory shows that the PDE has a damped character due to the sign of the linearized term that is proportional to $D_n - 1$. In the absence of $\dot{D}_n$, the PDE is classified as a parabolic PDE, which corresponds to the quasi-steady $D_n - \kappa$-relation found by setting $\dot{D}_n = 0$.

5.2.4. *Combined formulas:* $D \leq 1$

One can use the formulas (5.38) and (5.39) to construct a uniform composite approximation to the $\dot{D}_n - D_n - \kappa$- relation that is valid for D_n both near and below one. We replace $D_{,t}$ by $\dot{D}_n$ and rewrite (5.38) by

$$C_1(D)\dot{D}_n^2 + C_2(D)\dot{D}_n + C_3(D)\kappa = 0. \tag{5.49}$$

One can choose a value of $D \leq 1$ and κ, and then uses (5.49) to calculate $\dot{D}_n$; or assume a value of D and $\dot{D}_n$ and uses (5.49) to calculate κ. Then with the values of $\dot{D}_n$, κ and D fixed, one uses formula (5.29b) to calculate $\kappa D'$ and hence $D_n = D + \kappa D'$, thus generating a $(\dot{D}_n, D_n, \kappa)$-triad. Thus for a set of equation of state and kinetics parameters, one can generate plots of the $\dot{D}_n - D_n - \kappa$ - surface as well as contours in the

$D_n - \kappa$ plane for fixed $\dot{D}_n$ (say); albeit the required integrals that appear in the formulas must in general be done numerically.

The condition for hyperbolicity, that $(\partial\kappa/\partial\dot{D}_n)_{D_n} < 0$, must be checked, and the boundaries of this inequality form are used to discard spurious regions and identify the boundaries of the relation. In general, if we solve (5.49) for $\dot{D}_n$, we obtain

$$\dot{D}_n = -\frac{C_2}{2C_1}(1 - \sqrt{\Delta}), \quad \Delta = 1 - \frac{4C_1C_3\kappa}{C_2^2}. \tag{5.50}$$

We have selected the - branch for $\sqrt{\Delta}$, which is a choice consistent with the requirement of the analysis that $\dot{D}_n \sim o(1)$. Also, simply from the definitions of C_2 and C_3, one can show that in the limit as $D \to 1$, that both C_2, C_3 are finite and positive. Thus in an entire neighborhood of the surface with $D = 1$, these coefficients are positive. Also one can show that as $D \to 1$, $C_1 \to -\infty$. Thus the surface must contain the limiting point $\dot{D}_n = 0$, $D_n = 1$ and $\kappa = 0$ for $D = 1$. We take the implicit derivative of equation (5.49) with respect to $\dot{D}_n$, holding D_n fixed, (where D_n is approximated by D), and find

$$\frac{\partial\kappa}{\partial\dot{D}_n} = -\frac{C_2}{C_3}\sqrt{\Delta}. \tag{5.51}$$

Thus we find that the boundaries of the response surface (where the derivative changes sign), are defined by the conditions $C_2 = 0$, $C_3 = 0$, and $\Delta = 0$. For $D < 1$, Δ is strictly bounded from zero, and is approximated by $\Delta \sim 1$, for sufficiently small κ. However for $D \sim 1$, the boundary $\Delta = 0$ is described by $\kappa = C_2^2/4C_1C_3$.

5.3. *Examples for a condensed explosives and for gaseous explosives*

We display the $\dot{D}_n - D_n - \kappa$ - relation for two important cases; one that models a condensed explosive, and one that models a gaseous explosive mixture. The polytropic (ideal) equation of state is accurate in a quantitative sense only for gaseous mixtures. The use of the polytropic EOS for condensed explosives provides a useful, analytically tractable model that can generate the correct magnitudes for detonation speeds and states, however the equation of state in the unreacted explosive is poorly modeled. The condensed-phase model has been used by us in the past for the purpose of analytical testing of numerical schemes and qualitative predictions about detonation shock dynamics, Stewart & Bdzil (1991).

In order to generate model results for qualitative and numerical testing purposes for a representative condensed-phase explosive, it is important to choose parameters that reflect the reacted products behind the detonation shock and to display the results in physical units. Representative parameters are $\gamma = 3$, an initial density $\tilde{\rho}_0 = 2$ gm/cc, a heat of combustion $\tilde{Q} = 4 \times 10^6$ Joules/Kg. The corresponding CJ detonation speed, from the strong shock approximation shows $\tilde{D}_{CJ} = \sqrt{2(\gamma^2 - 1)\tilde{Q}} = 8$ Km/sec. The depletion parameter ν is chosen to be 1/2. The pre-multiplying rate constant $\tilde{k}$ controls the size of a steady 1/2-reaction length, but typically one chooses it to correspond to a typical reaction zone length in a condensed explosive, which can range from 1/10 to a few millimeters. The value $\tilde{k} = 2.5147\,\mu$sec corresponds to a steady half-reaction-zone length, $\tilde{\ell}_{1/2} = 1$ mm. When the activation-energy $\tilde{E}$ is taken to be zero, the rate integrals, I_1, I_2, J_1, J_2, J can be carried out analytically, and those exact integrals are listed in Appendix IV.

Figure 1 (a) shows a surface plot of the $\dot{D}_n - D_n - \kappa$ - relation, for the condensed explosive case ($\gamma = 3, \nu = 1/2, \theta = 0$), generated from the formulas of previous section.

The surface is plotted in a space that has D_n in the vertical - direction, κ in the horizontal x - direction, and $\dot{D}_n$ in the out of plane - direction. Contours of constant $\dot{D}_n$ are shown and labeled in the surface. For all the plots section, the 1/2-reaction length is used to scale the curvature.

The surface has a tent shape with a distinct fold near $D_n = 1$, which seperates the two branches of the surface, $D < 1$ and $D \sim 1$. The plane $\dot{D}_n = 0$, intersects the surface along the surface along the $D_n - \kappa$ -relation for $\kappa > 0$. Also the plane intersects the surface along the vertical line $\dot{D}_n = 0, \kappa = 0$ for all D_n. Thus in the surface, the contour $\dot{D}_n = 0$ has a discontinuous derivative exactly at $D_n = 1$. The segment of the surface that is related to the branch $D \sim 1$, is completely visible in the surface plot and can be reasonably well-fit by a plane given by the equation

$$63.6\,\dot{D}_n + (D_n - 1) + 8.35\,\kappa = 0. \tag{5.52}$$

The segment of the surface near $D_n = 1$ on the branch $D < 1$, is well-approximated by the $\dot{D}_n - \kappa$-relation given by (5.47). The surface is terminated by the view box on the left side of the plot. The lower portion of the surface is terminated by the view box. The left edge of the surface for $\kappa < 0$ correspond to the hyperbolic boundary $\Delta = 0$.

Figure 1(b) shows the projection of the surface onto the $D_n - \kappa$ - plane, with the contours of $\dot{D}_n$ indicated. For this case, where the activation energy is zero, increasing negative curvature is associated with decreasing values of D_n. This is not the case for large-activation-energy.

Figures 2(a,b) and figures 3(a,b) show a similar set of plots of the $\dot{D}_n - D_n - \kappa$-surface, for a gaseous equation of state with $\gamma = 1.2$. Figures 2(a,b) are drawn with zero activation-energy ($\theta = 0$), and a depletion factor $\nu = 1$. Figures 2(a,b) appear qualitatively similar to those of the condensed case (for $\gamma = 3$) shown in figures 1(a,b). In particular, we note that D_n decreases with increasing negative curvature in the neighborhood of $D_n = 1$. In contrast, figures 3(a,b) are drawn for a non-zero activation-energy with Erpenbeck's scaled activation-energy $E = 16$ ($\theta = 4/11$). One sees the appearance of both hyperbolic boundaries $C_2 = 0$ and $\Delta = 0$. The most striking difference is that D_n increases above 1 for negative κ in the neighborhood of $D_n = 1$. This property of the surface is preserved in the distinguished limit of large activation-energy considered in the next section.

6. The limit of large-activation-energy and small-curvature and slow-evolution

Here we seperately consider a distinguished limit of large-activation energy and small-curvature and slow-evolution. We derive the $\dot{D}_n - D_n - \kappa$ - relation under the assumption that the normal acceleration effects and the curvature effects modify the quasi-steady reaction-zone at the same order. For large-activation-energy the reaction-zone is an induction-zone, followed by a thin heat-releasing reaction-zone. This analysis follows our work in Yao & Stewart (1994), where we calculated the $D_n - \kappa$ - relation in the absence of the $\dot{D}_n$-terms. There we assume that the small-curvature is measured on a typical induction-zone length scale for the plane-CJ detonation, and is specifically $O(1/\theta)$ on that scale. Deviations of the normal detonation velocity of $O(D_n - 1)$ are assumed to be of the same order; and as a consequence, the analysis shows that the $D_n - \kappa$-relation is multi-valued in D_n for a limited range of κ, and that a critical pair $[(D_n)_{cr}, \kappa_{cr}]$ exists such that for $\kappa > \kappa_{cr}$, no asymptotic solution of this type exists.

By the arguments of section 5.2.1., the $D_n - \kappa$-relation (which is an intrinsic PDE for

the motion of the shock surface) is a parabolic PDE. For $D_n > (D_n)_{cr}$ and $0 < \kappa < \kappa_{cr}$, the slope, $\partial D_n/\partial\kappa < 0$ and the PDE is parabolic with a *positive* diffusion coefficient, hence the shock dynamics can be regarded as locally stable. However for $D_n < (D_n)_{cr}$, for $0 < \kappa < \kappa_{cr}$, the slope $\partial D_n/\partial\kappa > 0$, and the PDE is parabolic with a *negative* diffusion coefficient and the local dispersion relation shows the instability commonly associated with the backwards heat equation.

The effect of increasing the activation-energy θ in the formulas of section 5., does not show the evidence of the same turning point in the projected $D_n - \kappa$ plane. This is explained by the fact that the large-activation-energy limit there corresponds to the sequential limit $\theta \to \infty(\kappa \to 0)$. This limit thus, does not reflect the large changes that the curvature can have on an induction-zone which is sensitive to temperature perturbations. This is in contrast to the distinguished limit carried out in Yao & Stewart (1994), where the curvature scales with activation-energy, such that its effect is felt in the induction-zone. The distinguished limit considered here in section 6. leads to an explicit closed form of the $\dot{D}_n - D_n - \kappa$- relation which is expressed simply, and is tractable for further analysis. We present this relation as a model for the shock dynamics of near-CJ detonations that ultimately can describe certain features of the dynamics of cellular detonation, as we explain in section 7.

The distinguished limit can be described from the formulas of the previous section as follows. If we assume that D_n is close to one and that λ_{CJ} can be replaced by one, then (5.20) simplifies to

$$D_n = 1 - \gamma^2(I_1 - I_2)\kappa - [(\gamma^2 - 1)(I_1 + J_2) + \gamma^2(I_1 + J_1)]\dot{D}_n, \tag{6.1}$$

where the integrals I_1, I_2, J_1, J_2 are over the reaction-zone structure, from the shock to the sonic point. However due to the appearance of the reaction rate in the denominator of the integrand, the dominant contribution to the integrals comes near the shock, in the induction-zone, since there the reaction is the smallest. If the dynamics of the evolution is assumed to be such that shock acceleration terms occur at the same order as the curvature terms (which is our premise) then the integrals will depend on the normal acceleration as well. Evaluation of the contributions to the integrals from the normal acceleration terms, are then inserted back into (6.1) and the explicit form of the evolution equation is obtained. What follows next is a detailed derivation.

6.1. *Scaling*

The characteristic reaction-zone length is explicitly identified as the induction-zone length of the plane-CJ detonation, commensurate with the 1/2-reaction length found in the limit of large-activation-energy, $\tilde{\ell}_{rz} = \tilde{k}^{-1}\tilde{D}_{CJ}exp[\theta/c_s^2]/\theta$, where $c_s^2 = 2\gamma(\gamma - 1)/(\gamma + 1)^2$. Therefore the reaction rate is written as

$$r = \frac{(1-\lambda)^\nu}{\theta} exp[\theta(1/c_s^2 - 1/c^2)]. \tag{6.2}$$

We specifically assume evolution on time scale

$$\tau = \frac{t}{\theta}\,. \tag{6.3}$$

The curvature is assumed to be small on the induction length scale,

$$\kappa = \frac{\hat{\kappa}}{\theta}, \text{ where } \hat{\kappa} \sim O(1). \tag{6.4}$$

Note that the curvature is allowed to be a (slow) function of the transverse coordinate ξ (whose dependence is not shown) and the slow-time τ. The induction-zone is a zone of small-depletion, whose independent spatial variable is taken to be

$$z = \theta\lambda \quad . \tag{6.5}$$

Finally, we expand the detonation velocity D_n and the state as

$$\begin{aligned} D_n &= 1 + \kappa D'(\tau) + \tau\hat{D}(\tau) + \dots, \\ v &= \frac{\gamma-1}{\gamma+1} + \kappa v'(\tau, z) + \dots, \\ U &= -\frac{\gamma-1}{\gamma+1} + \kappa U'(\tau, z) + \tau\left[-\frac{\gamma-1}{\gamma+1}\hat{D}\right] + \dots, \\ p &= \frac{2}{\gamma+1} + \kappa p'(\tau, z) + \tau\left[\frac{4}{\gamma+1}\hat{D}\right] + \dots, \end{aligned} \tag{6.6}$$

and it follows that

$$c^2 = c_s^2 + \kappa(c^2)'(\tau, z) + \tau\left[4\hat{D}\frac{\gamma(\gamma-1)}{(\gamma+1)^2}\right] + \dots \quad . \tag{6.7}$$

The linearized shock conditions require that at $z = 0$

$$v'(\tau, 0) = 0, \;\; U'(\tau, 0) = -\frac{\gamma-1}{\gamma+1}D', \;\; p'(\tau, 0) = \frac{4}{\gamma+1}D'. \tag{6.8}$$

The expansions given by (6.6) reflect small corrections to the constant state behind the shock of order κ and τ. The induction-zone is assumed to subjected to a curvature perturbation and slow-acceleration of the same magnitude. The acceleration terms in the expansions (proportional to τ) are consistent with velocity changes induced by a slowly-accelerating shock. In particular, it follows from (6.6 a) that

$$D_{n,t} = \frac{\hat{D}}{\theta} \tag{6.9}$$

and

$$\frac{\partial v}{\partial t} = 0, \;\; \frac{\partial U}{\partial t} = -\frac{\hat{D}}{\theta}\frac{\gamma-1}{\gamma+1}, \;\; \frac{\partial p}{\partial t} = \frac{\hat{D}}{\theta}\frac{4}{\gamma+1}, \;\; \frac{\partial c^2}{\partial t} = 4\frac{\hat{D}}{\theta}\frac{\gamma(\gamma-1)}{(\gamma+1)^2}. \tag{6.10}$$

Given the scalings and expansion introduced above, one can obtain a closed system of two equations from the master equation and Bernoulli's equation for the velocity perturbation $U' = [U + (\gamma)/(\gamma+1)]/\kappa$ and the sound speed squared perturbation, $y \equiv \theta(c^2 - c_s^2)$. Note that in the induction-zone, to leading order the ratio of the curvature to the rate is given by

$$\frac{\kappa}{r} = \hat{\kappa}e^{-\theta(c^2-c_s^2)/c_s^4} = \hat{\kappa}e^{-y/c_s^4}, \tag{6.11}$$

and the master equation in the induction-zone becomes

$$\hat{\kappa}\frac{\partial U'}{\partial z} = -\frac{1}{2(\gamma+1)} + 2e^{-y/c_s^4}\left[2\hat{\kappa}\frac{\gamma(\gamma-1)}{(\gamma+1)^3} + 3\frac{(\gamma-1)}{(\gamma+1)^2}\hat{D}\right]. \tag{6.12}$$

Similarily Bernoulli's equation reduces to

$$-\frac{\gamma-1}{\gamma+1}\hat{\kappa}\frac{\partial U'}{\partial z}+\frac{1}{\gamma-1}\frac{\partial y}{\partial z}-\frac{1}{2(\gamma^2-1)}=2e^{-y/c_s^4}\frac{(\gamma-3)}{(\gamma+1)^2}\hat{D}. \tag{6.13}$$

From these two equations we can eliminate $\hat{\kappa}\partial U'/\partial z$ and obtain a single first order equation for y,

$$\frac{\partial y}{\partial z}=\alpha+\hat{\kappa}\beta e^{-y/c_s^4}, \tag{6.14}$$

where we identify

$$\alpha=\frac{\gamma(3-\gamma)}{2(\gamma+1)^2},\quad \hat{\kappa}\beta=4\frac{\gamma(\gamma-1)^3}{(\gamma+1)^4}\hat{\kappa}+8\frac{\gamma(\gamma-1)(\gamma-2)}{(\gamma+1)^3}\hat{D}. \tag{6.15}$$

At the shock, we have $y(0)=2c_s^2\theta(D_n-1)$.

The solution for y subject to the shock boundary condition is

$$y=\alpha z+c_s^4\ell n\left(\sigma-\hat{\kappa}\frac{\beta}{\alpha}e^{-\alpha z/c_s^4}\right), \tag{6.16}$$

where

$$\sigma-\hat{\kappa}\frac{\beta}{\alpha}=exp\left[\frac{(\gamma+1)^2}{\gamma(\gamma-1)}\theta(D_n-1)\right]. \tag{6.17}$$

What remains is integral asymptotics, applied to the integrals I_1, I_2, J_1 and J_2, which can be summarized as follows. Because of the appearance of the inverse reaction rate in the integrals, and since the rate is by assumption, exponentially large once appreciable reaction occurs, it follows that $J_1\sim 0$, and $I_1(\gamma+1)/2\sim(I_1-I_2)(\gamma+1)^2/4\sim -J_2(\gamma+1)^2/[4(\gamma-1)]\sim I$, where

$$I\equiv\int_0^1\frac{1}{r}d\lambda\sim\int_0^\infty e^{-y/c_s^4}dz. \tag{6.18}$$

Using the approximation for the sound speed squared perturbation for y in (6.16) then obtains

$$I=\frac{c_s^4}{\hat{\kappa}\beta}[\ln(\sigma)-\ln(\sigma-\hat{\kappa}\frac{\beta}{\alpha})], \tag{6.19}$$

Inserting these results back into (6.1) obtains the explicit evolution equation

$$\theta(D_n-1)=\frac{\mu}{\beta}[\ell n(\sigma)-\ell n(\sigma-\hat{\kappa}\frac{\beta}{\alpha})]. \tag{6.20}$$

where

$$\hat{\kappa}\mu=c_s^4[\hat{\kappa}\frac{4\gamma^2}{(\gamma+1)^2}+\frac{2(4\gamma-3)}{\gamma+1}\hat{D}]. \tag{6.21}$$

Now using the definitions of $\hat{\kappa}$ and $\hat{D}$, we rewrite (6.20) as

$$\kappa=\frac{\alpha}{\theta\beta}e^{(2/c_s^2-\beta/\mu)\theta(D_n-1)}[1-e^{(\beta/\mu)\theta(D_n-1)}], \tag{6.22}$$

where

$$\kappa\mu = c_s^4[\frac{4\gamma^2}{(\gamma+1)^2}\kappa + \frac{2(4\gamma-3)}{\gamma+1}\dot{D}_n], \tag{6.23}$$

and

$$\kappa\beta = 4\frac{\gamma(\gamma-1)^3}{(\gamma+1)^4}\kappa + 8\frac{\gamma(\gamma-1)(\gamma-2)}{(\gamma+1)^3}\dot{D}_n. \tag{6.24}$$

Note that when $\dot{D}_n$ is absent, we obtain the $D_n-\kappa$-relation, calculated in Yao & Stewart (1994).

$$\kappa = \frac{e^{b\theta(D_n-1)}}{d\theta}(1-e^{a\theta(D_n-1)}), \tag{6.25}$$

where

$$a = \left(\frac{\beta}{\mu}\right)_{\dot{D}_n=0} = \frac{(\gamma+1)^2(\gamma-1)}{4\gamma^3},\ b = \frac{2}{c_s^2} - a = \frac{(\gamma+1)^3(3\gamma-1)}{4\gamma^3(\gamma-1)}, \tag{6.26}$$

and

$$d = \frac{8(\gamma-1)^3}{(3-\gamma)(\gamma+1)^2}. \tag{6.27}$$

Figures 5(a,b) show two representations of the $\dot{D}_n - D_n - \kappa$ - relation in the limit of large-activation-energy. Figure (5a) shows a surface plot of the surface in the $\dot{D}_n - D_n - \kappa$ - space, and figure (5b) shows $D_n - \kappa$ curves taken at different values of $\dot{D}_n$.

It can be shown that the evolution equation (6.22) is hyperbolic. In addition at a point on the surface where $\partial D_n/\partial\kappa|_{\dot{D}_n} < 0$, the dispersion relation corresponds to stable growth of local disturbances, while for $\partial D_n/\partial\kappa|_{\dot{D}_n} > 0$, corresponds to unstable growth of local disturbances. The dispersion relation derived from the frozen coefficient analysis only yields information about character of the evolution for short time, from some assumed initial configuration of the detonation shock and does not predict the consequence of the nonlinear evolution. However the instability indicated, corresponds to a situation where the detonation shock experiences positive normal acceleration in the presence of positive curvature. One can envision circumstances where a convex portion of the detonation shock, which has normal velocity below D_{CJ}, accelerates and becomes more highly convex, and we have seen that property in the numerical solutions to (6.22).

7. Numerical experiments

Here we present the results of some two-dimensional numerical experiments and comparisons that use $\dot{D}_n - D_n - \kappa$ - relations. The numerical solution of the intrinsic PDEs shown here were carried out in collaboration with T. Aslam, and employ a level-set technique that follows the work of Osher & Sethian (1988). The numerics are described briefly in Stewart, Aslam, Yao & Bdzil (1994), and will be discussed seperately, in subsequent papers. The main points to be demonstrated here, concern the qualitative differences between the detonation shock dynamics predicted by a $\dot{D}_n - D_n - \kappa$-relation and those corresponding to a $D_n - \kappa$-relation, and their prediction of detonation shock dynamics observed in physical experiments.

7.1. *Differences between hyperbolic and parabolic evolution*

Our first example illustrates the qualitative difference between the hyperbolic $\dot{D}_n - D_n - \kappa$-relation and the corresponding parabolic $D_n - \kappa$-relation, for the parameters of the condensed phase model, discussed in Section 5.3. and illustrated in Figure 1(a) and (b). We restrict attention to the branch of the response surface for $D \sim 1$, approximated by (5.52). We display the results of the first numerical experiment, in length and time unit of millimeters (mm) and microsec μsec, respectively, and in these units (5.52) becomes

$$\tilde{D}_n = 8 - 66.8\tilde{\kappa} - 7.95\dot{\tilde{D}}_n \ , \tag{7.1}$$

with the corresponding $D_n - \kappa$-relation

$$\tilde{D}_n = 8 - 66.8\tilde{\kappa} \ . \tag{7.2}$$

A slab with a half-width of 50 mm and length of 400 mm was used for the experiments. At time t = 0, a plane, CJ-shock is assumed at $x = 0$ mm. Solutions for the shock dynamics in finite domains, require boundary conditions to be applied at edges for all time. At the bottom edge (y = 0 mm), we assumed an angle boundary condition, and in particular the angle between the outward normal of the confining edge and the normal to the shock was taken to be 45 degrees. At the top edge (y = 50 mm), the confinement was assumed to be perfect and corresponds to a symmetry (or reflection boundary conditions), and the angle between the outward normal of the confining edge and the normal to the shock was set to 90 degrees.

Figures 6(a,b) show combined contour and line plots that show features of the numerical solution the initial-boundary value problem defined above. Figure 6(a) corresponds to a numerical solution of the $D_n - \kappa$ -relation defined by (7.2) and figure 6(b) corresponds to that defined by (7.1). The different grayscale contours, separated by lines that run roughly along the axis of the slab, indicate the value of the detonation velocity recorded at a fixed Eulerian point in the slab, at the time that the detonation shock crosses the point. Dark regions correspond to lower normal detonation velocity and lighter regions higher values. The shock positions also shown at various times, at equal time intervals of 3.6 μ sec, and cut transversely to the lines of constant $\tilde{D}_n$.

The most obvious difference between the two simulations, is illustrated by the relaxation towards an axial steady state, of an initial plane-CJ shock, in response to the edge boundary condition applied at y = 0 mm. The relaxation of the solution $D_n - \kappa$- relation from plane- CJ to its axial, steady-state in response to a step change in slope, is via local, self-similar relaxation, characteristic of the heat equation. This is seen in the curves of constant $\tilde{D}_n$ where, $y \sim \sqrt{x}$. In contrast, the hyperbolic character of solution to (7.1) is seen by the curves of constant $\tilde{D}_n$ with, $y \sim x$, that is the consequence of the self-similarity of the local wave equation that governs in the early transient. Also for the example shown, the relaxation for the $D_n - \kappa$-relation, shown in figure 6(a), is accomplished quickly in the first 100 mm (say), while an obvious transient still persists in the solution of the $\dot{D}_n - D_n - \kappa$-relation, even at 400 mm, four slab thicknesses wide. The constant D_n contours show the evidence of multiple wave reflections of the initial disturbance off the confinement boundaries. The shapes of the axial, steady shock loci are different in the two cases, which is due to the effects of the normal acceleration, $\dot{D}_n$.

7.2. *Aspects of detonation cells*

Our second example, draws from our experience developed in carrying out numerical solutions to (6.22). But first we mention some aspects of the observations of multi-dimensional detonation cells, seen in experimental systems, such as those observed by

Strehlow Liaugminas Watson & Eynman (1967), in dilute Hydrogen-Oxygen explosive mixtures. In a typical experiment, a long, rectangular channel is used to contain an unreacted, explosive mixture of Hydrogen/Oxygen gas, diluted by Argon (say). The mixture is ignited at a closed-end and is allowed to propagate down the tube. As it propagates, the detonation shock, instead of being plane, has a set of disjoint cells, which are made up of segments of the detonation shock that travel at different normal velocities, and correspond to quite different shock pressures. The segments of the detonation shock are resolved by shock/shock interactions that may be regular, or may lead to Mach-stem formation and growth. In the case of a regular reflection, the triple point maintains, while in the case of Mach-stem growth, the point of interaction becomes two triple points connected by a bridge that grows in width. Thus the cellular detonation shock front can be characterized simply as a network of triple points that are connected to smooth shock fronts.

In the physical experiment, the inside of the tube is lined with a foil that is covered with a soot, typically from kerosene burned in air, which is scraped away by the high pressure detonation shock that intersects the tube wall. In particular, the loci of the wall motion of the triple points is easily recorded in this technique, since they are associated with the highest pressures in the flow.

A conjecture we made, was that numerical solutions to (6.22), might show evidence of a *self-sustained* cellular detonation front, similar to those seen in the experiment described above. Then a single evolution equation, necessarily of hyperbolic character, could be used to describe the motion of the cellular detonation front. The attempt at this time to verify this conjecture is incomplete, especially in regards to the question as to whether the cellular solutions of (6.22) are self-sustained. It is likely that modifications to (6.22) are required that included faster transients, and that (6.22) contains the leading terms in an appropriate expansion. But we have been able to verify that certain aspects of cellular behavior are found.

Our experience in working with (6.22), shows that it apparently admits weak solutions with continuity of the shock locus, but with discontinuities in the shock slope. The points of the intersection, where the shock slope is discontinuous, between different, otherwise smooth shock segments, then would correspond to the location of triple points, in an experiment. In our numerical experiment, the channel was hundred of units long and wide, measured in half-reaction lengths. The side walls of the channel were assumed to be reflecting. Typically we took the initial shape of the shock to be a sine wave in the width. It is necessary to give the initial velocity of the wave, for the hyperbolic PDE, and in most of our experiments we took D_n to be one or less than one. The subsequent evolution was calculated numerically. At each point in the domain of the channel, the value of the arrival time of the shock and the value of D_n was recorded, similar to that in the first experiment.

The transient evolution, found in the numerical experiments, displayed many features that are common to cellular detonation. In particular, as the shock evolved from the sinusoidal initial data, it quickly formed sharp shock/shock cusps at points that would correspond to triple points. These points moved side to side on the shock front as the shock moved forwards. When the triple points collided with the side wall, they were reflected back into the channel, as would be expected in the physical experiment. For many of the experiments we tried, cells would form quickly and the number of cells, (counted from the patterns that the triple points made as they propagated down the channel), would persist. However by varying the spatial frequency of the initial sinusoidal shape of the shock and the initial velocity, we did find cases where the frequency of the

initial data was not preserved. In these cases, cells quickly merged and were absorbed by larger cells, that then persisted.

We also found that the shock complex would flatten in time and we suspect that the solution may ultimately dissipate to nearly a plane wave, moving at $D_n = 1$, in the limit of large time. This issue however is not trivially resolved by increasing the numerical resolution, and is still under investigation. Thus our question of self-sustainabililty is not resolved and the evolution predicted by (6.22) may only need to be modified to describe such behavior.

Also as a test, we tried to roughly match the aspect ratio of the cells seen in physical experiments, with those of the simulation. We could do this if we took an artificially high value of $\gamma = 1.9$ and a very large-activation-energy. But even then the transverse wave speed of the triple points (which can be calculated approximately from a linear analysis of (6.22), produced cells that were quite long, compared to representative physical experiment, with aspect ratios of length to width of 2 or more. One difficulty in making this comparison directly from solutions to (6.22), is the use of the strong shock approximation, which strictly breaks down as $\gamma \to 1$. Thus we might not expect our formulas to be very accurate for realistic values of $\gamma = 1.2$ or 1.4. We have not precisely reproduced the geometry of the physical experiment and included fully accounted for three-dimensional effects of the experiment, in order to make the comparisons.

We also observed that when we found cell-like behavior, that most of the time, the shock sampled the $\dot{D}_n - D_n - \kappa$-relation where it was approximately described by a simpler $\dot{D}_n - \kappa$-relation. And we were able to verify that one could generate qualitatively similar solutions, whose triple points made similar patterns to those generated for (6.22) with a simple $\dot{D}_n - \kappa$-relation. Figure 7 shows the result of a numerical solution of a dimensionless $\dot{D}_n - \kappa$-relation, given by

$$\dot{D}_n = -(0.65)^2 \kappa, \tag{7.3}$$

in a channel 400 wide and 700 long. The initial shock position was taken to be $x_{shock} = 20[1 + cos(2\pi y/100)]$. The initial shock velocity was taken to be $D_n = 1$. We varied the constant of proportionality of a $\dot{D}_n - \kappa$-relation $(0.65)^2$ so as to control the observed cell aspect ratio and make it match a cell-pattern in Strehlow Liaugminas Watson & Eynman (1967). Figure 7 shows a combined contour and line plots that show features of the numerical solution to the initial-boundary value problem defined above. The grayscale contours indicate the value of the detonation velocity recorded at a fixed Eulerian point in the slabs, at the time that the detonation shock crosses the point. Dark regions correspond to lower normal detonation velocity and lighter regions higher values. The shock position are shown as broken lines at at equal time intervals. The triple points of the solution, defined by the intersection of connected shocks that form the shock surface, form in the vicinity of $x = 50$ and subsequently trace out the diamond-spade patterns on the side of confining walls, like those that are recorded on smoke-foil records taken in experiments in gases, when cellular detonation is observed.

8. Appendix I: Betrand-Intrinsic Coordinates

The shock surface can be represented quite generally in terms of laboratory-fixed coordinates (x, y) as $\psi(x, y, t) = 0$. This equation constrains the lab-coordinate position vectors in the surface to $\vec{x} = \vec{x}_s$. The normal to the surface is chosen to be positive in the direction of the unreacted explosive and can always be calculated by the formula $\hat{n} = \vec{\nabla}\psi/|\vec{\nabla}\psi|$. The shock surface can be represented by a surface parameterization

$\vec{x} = \vec{x}_s(\xi, t)$, where ξ measures length along the coordinate lines of the surface. The unit vector in the shock surface, tangent to it, is defined by $\hat{t} \equiv \partial \vec{x}_s / \partial \xi$. The total curvature of the surface is given by $\vec{\nabla} \cdot \hat{n} = \kappa(\xi, t)$. For the present purpose, it is sufficient to assume that a straight line intersects the shock surface, and that the intersection point defines the instantaneous origin for the intrinsic coordinate system.

The intrinsic coordinates are related to the laboratory coordinates by the change of variable given by

$$\vec{x} = \vec{x}_s(\xi, t) + n\,\hat{n}(\xi, t), \tag{8.1}$$

The Frenet formulas in 2D are

$$\frac{\partial \hat{t}}{\partial \xi} = -\kappa \hat{n}, \quad \frac{\partial \hat{n}}{\partial \xi} = \kappa \hat{t}. \tag{8.2}$$

and reflect the fact the intrinsic coordinate system is locally orthogonal.

Notice that in 2D, one can define the angle, ϕ between the edge line and the normal $\hat{n}$, and the derivative of the angle ϕ, with respect to the arclength ξ defines the curvature $\kappa = \partial\phi / \partial\xi$. Then normal and tangent unit vectors are related to the Cartesian basis by $\hat{n} = sin(\phi)\hat{e}_x + cos(\phi)\hat{e}_y$, $\hat{t} = cos(\phi)\hat{e}_x - sin(\phi)\hat{e}_y$. It is a straightforward matter to relate arclength, angle coordinates to laboratory coordinates.

The equations of motion are transformed from a representation in (x,y,t)-coordinates to (n, ξ, t)-coordinates according to coordinate transformation (8.1). The calculations required are straightforward but lengthy. Here we give the essential results needed. More details can be found in Lee, J (1992), Stewart (1993) and Yao (1995). In what follows, in regards to fixed quantities in partial differentiation, $\vec{x}$ refers to (x, y), and $\vec{\zeta}$ refers to (ξ, n).

The $\vec{\nabla}$ operator is given by

$$\vec{\nabla} = \hat{t} \frac{1}{1 + n\kappa} \frac{\partial}{\partial \xi} + \hat{n} \frac{\partial}{\partial n}. \tag{8.3}$$

By using the definition of the velocity in the intrinsic coordinates $\vec{u} = u_\xi \hat{t} + u_n \hat{n}$, we calculate the divergence $\vec{\nabla} \cdot \vec{u}$, and $\vec{u} \cdot \vec{\nabla}$ as

$$\vec{\nabla} \cdot \vec{u} = \frac{\partial u_n}{\partial n} + \frac{1}{1 + n\kappa} \left[\kappa u_n + \frac{\partial u_\xi}{\partial \xi} \right], \quad \vec{u} \cdot \vec{\nabla} = \frac{u_\xi}{1 + n\kappa} \frac{\partial}{\partial \xi} + u_n \frac{\partial}{\partial n}. \tag{8.4}$$

The time derivative in the lab-fixed coordinates is related to that in the shock-attached coordinates by $(\partial/\partial t)_{\vec{x}} = (\partial/\partial t)_{\zeta} + (\partial n/\partial t)_{\vec{x}} (\partial/\partial n) + (\partial \xi/\partial t)_{\vec{x}} (\partial/\partial \xi)$, where $(\partial n/\partial t)_{\vec{x}} \equiv -D_n$ is the negative of the normal component of the shock surface velocity and, $(\partial \xi/\partial t)\vec{x} \equiv B$, when evaluated at $n = 0$, is the instantaneous rate of increase or decrease of arclength along the shock. Thus we write

$$\left(\frac{\partial}{\partial t} \right)_{\vec{x}} = \left(\frac{\partial}{\partial t} \right)_{\vec{\zeta}} - D_n \frac{\partial}{\partial n} + B \frac{\partial}{\partial \xi}. \tag{8.5}$$

Next we derive the *kinematic relations* which gives a differential condition on B, in particular, which we later use to estimate the asymptotic order of certain terms in the transformed equations, for small curvature. Differentiating the change of variable formula (8.1) with respect to t, holding $\vec{x}$- fixed (and using the chain rule and Frenet formulas) obtains,

$$\left(\frac{\partial \vec{x}_s}{\partial t}\right)_{\vec{\zeta}} + n\left(\frac{\partial \hat{n}}{\partial t}\right)_{\vec{\zeta}} - D_n\hat{n} + \left(\frac{\partial \xi}{\partial t}\right)_{\vec{x}}(1+n\kappa)\hat{t} = 0. \tag{8.6}$$

Next we differentiate (8.6) with respect to ξ, holding n and t -fixed, and use the Frenet formulas to obtain a vector equation, whose $\hat{n}$ and $\hat{t}$ - components are

$$\hat{n}\cdot\left(\frac{\partial \hat{t}}{\partial t}\right)_{\vec{\zeta}} - \kappa\left(\frac{\partial \xi}{\partial t}\right)_{\vec{x}} - \frac{\partial D_n}{\partial \xi}\frac{1}{1+n\kappa} = 0, \tag{8.7}$$

$$\frac{\partial}{\partial \xi}\left[(1+\eta\kappa)\left(\frac{\partial \xi}{\partial t}\right)_{\vec{x}}\right] + n\frac{\partial \kappa}{\partial t} = \kappa D_n. \tag{8.8}$$

Equation (8.7) can be further simplified. By differentiating (8.7) by ξ, and by using the result that $\partial/\partial\xi[\hat{n}\cdot(\partial\hat{t}/\partial t)_{\vec{\zeta}}] = -\partial\kappa/\partial t$, one obtains an expression for $\partial\kappa/\partial t$. Then using that formula in (8.8), one obtains the simple expression

$$\frac{\partial}{\partial \xi}\left[\left(\frac{\partial \xi}{\partial t}\right)_{\vec{x}} - \frac{n}{1+n\kappa}\frac{\partial D_n}{\partial \xi}\right] = \kappa D_n. \tag{8.9}$$

In particular, (8.9) can be used to estimate the size of $B = (\partial\xi/\partial t)_{\vec{x}}$.

When specialized to the surface $n = 0$, the kinematic relations (8.7) and (8.9) describe the evolution of the surface, itself and reduce to the *kinematic surface relations*

$$\frac{\partial}{\partial \xi}\left[\left(\frac{\partial \xi}{\partial t}\right)_{\vec{x}}\right] = \kappa D_n, \quad \left(\hat{n}\cdot\frac{\partial \hat{t}}{\partial \xi}\right)_{\vec{\zeta}} - \left(\frac{\partial \xi}{\partial t}\right)_{\vec{x}} = \frac{\partial D_n}{\partial \xi}. \tag{8.10}$$

9. Appendix II: Reduced Governing Equations

The governing equations in Bertrand-intrinsic coordinates follow from a straightforward application of the formulas of Appendix I. If we define $U_n = u_n - D_n$, the governing equations are written as:

$$\frac{\partial \rho}{\partial t} + \frac{\partial}{\partial n}(\rho U_n) = -\kappa\frac{\rho(U_n + D_n)}{1+n\kappa} - R_1, \tag{9.1}$$

$$\frac{\partial U_n}{\partial t} + \dot{D}_n + U_n\frac{\partial U_n}{\partial n} + \frac{1}{\rho}\frac{\partial p}{\partial n} = -R_2, \tag{9.2}$$

$$\frac{\partial u_\xi}{\partial t} + U_n\frac{\partial u_\xi}{\partial n} = -R_3, \tag{9.3}$$

$$\frac{\partial e}{\partial t} + U_n\frac{\partial e}{\partial n} - \frac{p}{\rho^2}\left(\frac{\partial \rho}{\partial t} + U_n\frac{\partial \rho}{\partial n}\right) = -R_4, \tag{9.4}$$

$$\frac{\partial \lambda}{\partial t} + U_n\frac{\partial \lambda}{\partial n} = r - R_5, \tag{9.5}$$

where

$$R_1 = \frac{\rho}{1+n\kappa}\frac{\partial(\rho u_\xi)}{\partial \xi} + \left[\frac{u_\xi}{1+n\kappa} + B\right]\frac{\partial \rho}{\partial \xi}, \tag{9.6}$$

$$R_2 = \left[\frac{u_\xi}{1+n\kappa} + B\right]\frac{\partial u_n}{\partial \xi} - u_\xi^2\frac{\kappa}{1+n\kappa} + B\frac{\partial U_n}{\partial \xi} - Bu_\xi\kappa, \tag{9.7}$$

$$R_3 = \left[\frac{u_\xi}{1+n\kappa} + B\right]\frac{\partial u_\xi}{\partial \xi} + u_\xi(u_n)\frac{\kappa}{1+n\kappa} + Bu_n\kappa + \frac{1}{\rho}\frac{1}{1+n\kappa}\frac{\partial p}{\partial \xi}, \tag{9.8}$$

$$R_4 = \left[\frac{u_\xi}{1+n\kappa} + B\right]\left[\frac{\partial e}{\partial \xi} - \frac{p}{\rho^2}\frac{\partial \rho}{\partial \xi}\right], \tag{9.9}$$

$$R_5 = \left[\frac{u_\xi}{1+n\kappa} + B\right]\frac{\partial \lambda}{\partial \xi}. \tag{9.10}$$

Notice that in equation (9.2), that $\dot{D}_n \equiv (\partial D_n/\partial t)_{\vec{\xi}} + B\partial D_n/\partial \xi$, appears explicitly, which is the intrinsic time derivative of D_n along the shock normal.

In addition, it is necessary to write down two independent energy equations, that can be used to replace the n-momentum and energy equations respectively; these are essentially a streamwise Bernoulli's equation and what has been called the *master equation*, Bdzil (1981). Bernoulli's equation is given by

$$\begin{aligned}\frac{\partial}{\partial n}\left[\frac{U_n^2}{2} + \frac{1}{\gamma-1}c^2 - q\lambda\right] &= -\left(\frac{\partial U_n}{\partial t} + \dot{D}_n\right)\\ -\frac{1}{U_n}\left[\frac{1}{\gamma-1}\frac{1}{\rho}\frac{\partial p}{\partial t} - \frac{p}{\rho^2}\frac{\gamma}{\gamma-1}\frac{\partial \rho}{\partial t} - q\frac{\partial \lambda}{\partial t}\right] &- R_2 - \frac{R_3}{U_n}\end{aligned} \tag{9.11}$$

The master equation is written as

$$(c^2 - U_n^2)\frac{\partial U_n}{\partial n} = qr(\gamma-1) - \kappa\frac{c^2(U_n + D_n)}{(1+n\kappa)} + U_n\left(\frac{\partial U_n}{\partial t} + \frac{\partial D_n}{\partial t}\right) - v\frac{\partial p}{\partial t} + R, \tag{9.12}$$

where $R = -[\gamma p R_1 - uR_2 + (\gamma-1)(R_4 + qR_5)]$.

Next we argue for the form of the reduced equations, that for our needs, must be valid in the asymptotic sense in a region near the shock $n \leq 0$ with $n \sim O(1)$, as the shock curvature $\kappa \to 0$. Specifically we consider the size of the terms that comprise R_1 through R_5.

We assume that the dimensionless shock curvature, is small. Let the order of magnitude of the curvature be measured by ϵ^2, where $0 < \epsilon << 1$. We also assume that transverse spatial variation of the structure of the flow field behind the shock is weak, and is characterized by the scaled transverse variable,

$$\zeta = \epsilon\xi. \tag{9.13}$$

Therefore in the governing equations we assume that $\partial/\partial\xi = \epsilon\partial/\partial\zeta = O(\epsilon)$.

It follows from (8.9), and from the estimates $D_n \sim O(1)$, $\kappa \sim O(\epsilon^2)$, that one obtains an estimate for $B = (\partial\xi/\partial t)_{\vec{x}} \sim O(\epsilon)$. If one first supposes that $u_\xi \sim O(\epsilon)$ and $\partial p/\partial\xi \sim o(\epsilon)$, then R_3 is $o(\epsilon)$. Equation (9.3), with $R_3 = 0$, is the $O(\epsilon)$ equation for u_ξ, which can be integrated on its characteristic. Combined with the shock boundary condition that $u_\xi = 0$ at $n = 0$, one find that $u_\xi = 0$ to $O(\epsilon)$. Thus we are led to finer estimate that $u_\xi \sim o(\epsilon)$.

The terms R_1 through R_5 are $o(\epsilon^2) = o(\kappa)$, if one makes the modest assumption that

$$\frac{\partial \rho}{\partial \xi} \sim o(\epsilon), \quad \frac{\partial U_n}{\partial \xi} \sim o(\epsilon), \quad \frac{\partial p}{\partial \xi} \sim o(\epsilon), \quad \frac{\partial \lambda}{\partial \xi} \sim o(\epsilon), \tag{9.14}$$

which can be guaranteed, given the previous assumption on the explicit scaling for ξ, for any expansion of the reaction-zone structure where the $O(1)$ terms are not functions of ξ, and hence functions of at most n and t.

Note that no assumptions have been made so far, regarding the asymptotic nature of the time variation, and its relation to the order of κ. However, if we further assume, that we have slow-time variation in the shock-attached frame, and make only the assumption that $(\partial/\partial\xi)_{\vec{\zeta}} \sim o(1)$, then the intrinsic derivative $\dot{D}_n$ is approximated as $(\partial D_n/\partial t)_{\vec{\zeta}} + o(\kappa)$.

10. Appendix III: Limiting form of the steady $D_n - \kappa$ - relation

Here we consider only the integral asymptotics of the result stated in section 4., in the limit as $\nu \to 1$. Let

$$\lambda_{CJ} = 1 - (z^*\kappa)^{1/\nu}, \tag{10.1}$$

and D_n given by

$$D_n = 1 - \frac{1}{2}(z^*\kappa)^{1/\nu} - \kappa\gamma^2 I, \tag{10.2}$$

where

$$I \equiv I_1 - I_2 = \frac{1}{(\gamma+1)^2}\int_0^{\lambda_{CJ}} \frac{(1+\ell)^2}{r} d\lambda, \tag{10.3}$$

where $\ell = \sqrt{1-\lambda}$. Note that in order to properly calculate the contribution to the integral I, when $\nu \to 1$, one breaks the integral from 0 to λ into a contribution from 0 to 1 and 1 to λ_{CJ}. Hence for $\nu < 1$, one does the second integral, and combines the result to obtain in the formula for D_n

$$D_n = 1 - \kappa\frac{\gamma^2}{(\gamma+1)^2}\int_0^1 \frac{(1+\ell)^2}{r} d\lambda + \frac{\nu}{2(1-\nu)}(z^*\kappa)^{1/\nu} + o(\kappa^{1/\nu}). \tag{10.4}$$

For the case that $\nu = 1$, we can also get a formula with logarithmic contribution that is identical the result in Stewart & Bdzil (1988), Klein & Stewart (1993). To demonstrate this, without loss of generality, we take the rate multiplier to be equal to 1, and let $c^2(\ell) = \gamma(1+\ell)(\gamma-\ell)/(\gamma+1)^2$, write the result above as

$$\begin{aligned} D_n = 1 &- \kappa\frac{\gamma^2}{(\gamma+1)^2}\int_0^1 (1+\ell)^2(1-\lambda)^{-\nu}(e^{\theta/c^2} - e^{\theta/c^2(0)})d\lambda \\ &- \frac{\kappa z^*}{2}\int_0^1 \left((1+\ell)^2 - 1\right)(1-\lambda)^{-\nu} d\lambda - \frac{1}{2}\left[\frac{z^*\kappa}{1-\nu} - \frac{\nu(z^*\kappa)^{1/\nu}}{1-\nu}\right]. \end{aligned} \tag{10.5}$$

Now we evaluate the last two terms: The term

$$\frac{1}{2}\int_0^1 ((1+\ell)^2 - 1)(1-\lambda)^{-\nu} d\lambda = \frac{1}{4-2\nu} + \frac{2}{3-2\nu}, \tag{10.6}$$

with $\nu = 1$, is equal to $5/2$.

We also rewrite

$$\frac{1}{2}\left(\frac{z^*\kappa}{1-\nu}-\frac{\nu(z^*\kappa)^{1/\nu}}{1-\nu}\right)=\frac{1}{2}\left[(z^*\kappa)^{1/\nu}+\frac{z^*\kappa-(z^*\kappa)^{1/\nu}}{1-\nu}\right], \tag{10.7}$$

which can be evaluated with L'Hospital's rule as $\nu \to 1$, and which generates a logarithm.

Finally we obtain

$$D_n = 1-\kappa\left[3z^*+\frac{\gamma^2}{(\gamma+1)^2}\int_0^1 (1+\ell)^2(1-\lambda)^{-\nu}(e^{-\theta/c^2}-e^{-\theta/c^2(0)})d\lambda\right]+\frac{1}{2}z^*\kappa\ell n(z^*\kappa). \tag{10.8}$$

11. Appendix IV: The integrals with the simplest rate law (zero activation-energy

First we calculate the integrals for $D=1$ and $r\equiv(1-\lambda)^\nu$:

$$I_1=\frac{1}{(\gamma+1)}\left(\frac{1}{1-\nu}+\frac{2}{3-2\nu}\right), \tag{11.1}$$

$$I_2=\frac{1}{(\gamma+1)^2}\left(\frac{\gamma}{1-\nu}+\frac{2(\gamma-1)}{3-2\nu}-\frac{1}{2-\nu}\right) \tag{11.2}$$

$$I_3=\frac{1}{(\gamma+1)^2}\left(\frac{2\gamma}{(3-2\nu)}-\frac{1}{(2-\nu)}\right), \tag{11.3}$$

$$I_4=\frac{2}{(3-2\nu)}. \tag{11.4}$$

Note that integral J doesn't contribute to $G(D)$ when $D=1$, because that $r_{CJ}=0$.

For the case that D is away from 1 ,to calculate those integrals, we first define some simpler integrals, with $\ell\equiv\sqrt{1-\lambda/D^2}$

$$K_0=2D^2\int_0^1\frac{1}{r}d\ell,\quad K_1=2D^2\int_0^1\frac{\ell}{r}d\ell,\quad K_2=2D^2\int_0^1\frac{\ell^2}{r}d\ell,\quad K_3=2D^2\int_0^1\frac{\ell^3}{r}d\ell, \tag{11.5}$$

For $r=(1-\lambda)^\nu=(1-D^2+\ell^2D^2)^\nu$, we have:

$$K_0=\frac{2D^2}{(1-D^2)^\nu}F[1/2,\nu,3/2,D^2/(D^2-1)], \tag{11.6}$$

$$K_1=\frac{1}{1-\nu}(1-(1-D^2)^{1-\nu}), \tag{11.7}$$

$$K_2=\frac{2}{3D}(1-D^2)^{3/2-\nu}F[3/2,\nu,5/2,D^2/(D^2-1)], \tag{11.8}$$

$$K_3=\frac{1}{D^2}\left(\frac{1-(1-D^2)^{2-\nu}}{2-\nu}-(1-D^2)\frac{1-(1-D^2)^{1-\nu}}{1-\nu}\right), \tag{11.9}$$

where $F(a,b,c,z)$ is the hypergeometic function defined by the series

$$F(a,b,c,z)=\frac{\Gamma(c)}{\Gamma(a)\Gamma(b)}\sum_{n=0}^{\infty}\frac{\Gamma(a+n)\Gamma(b+n)}{\Gamma(c+n)}\frac{z^n}{n!}. \tag{11.10}$$

Thus we obtain

$$I_1 = \frac{1}{\gamma+1}(K_1 + K_2), \tag{11.11}$$

$$I_2 = \frac{1}{(\gamma+1)^2}(\gamma K_1 + (\gamma-1)K_2 - K_3), \tag{11.12}$$

$$I_3 = \frac{1}{(\gamma+1)^2}(\gamma K_2 - K_3), \tag{11.13}$$

$$I_4 = K_2 \tag{11.14}$$

$$J = \frac{1}{\gamma+1}(K_0 - \gamma K_1). \tag{11.15}$$

Acknowledgments

This work has been supported by the United States Air Force (USAF), Wright Laboratory, Armament Directorate, Eglin Air Force Base, F08630-92- K0057, and with computing resources from the National Center for Supercomputing Applications at the University of Illinois. Additional student support was made available through the USAF Office of Scientific Research, AASERT grant F49620-93-1-0532. Thanks to Tariq Aslam, for his assistance in carrying out the solutions to the numerical experiments discussed in section 7.

REFERENCES

BDZIL, J. B. 1981 Steady state two-dimensional detonation *Journal of Fluid Mechanics* Vol. 108, 1981, pp. 185-226.

BDZIL, J. B. & STEWART, D. S. 1988 Modeling of two- dimensional detonation with detonation shock dynamics. *Physics of Fluids*, A, Vol. 1, No. 7, 1261-.

ERPENBECK, J. J. 1964 The stability of idealized one dimensional detonations. *Phys. Fluids* 7:684-696

KLEIN, R. AND STEWART, D. S. 1993 The relation between curvature and rate state-dependent detonation velocity. *SIAM Journal of Applied Mathematics*, Vol. 53, No. 5, pp. 1401-1435.

JIE MIN'S 1990 PhD. thesis, Materials and Metallurgical Eng. New Mexico Institute of Mining and Technology, Soccoro, NM

OSHER AND SETHIAN 1988 Fronts propagating with curvature-dependent speed: Algorithms based on Hamiliton-Jacobi formulations. *Journal of Computational Physics*, 79, 12-49

STEWART, D. SCOTT 1993 Lectures on detonation physics: Introduction to the theory of detonation shock dynamics TAM report, No 721. UILU-ENG-93-6019.

STEWART, D. SCOTT, ASLAM, T. D., YAO, J. & BDZIL J. B. 1994 Level-set techniques applied to unsteady detonation propagation to appear in *Modeling in Combustion Science* (eds. J. Buckmaster & T. Takeno), Lecture Notes in Physics, Springer-Verlag pub, also appears as TAM report, N0.773, UIUC-ENG-94-6029, University of Illinois, Oct. 1994.

STEWART, D. S. & BDZIL, J. B. 1988 The shock dynamics of stable multi-dimensional detonation. *Combustion and Flame*, 72, 311-323.

STEWART, D. S. & BDZIL, J. B. 1993 Asymptotics and multi-scale simulation in a numerical combustion laboratory in *Asymptotic and numerical methods for partial differential equations with critical parameters, NATO ASI series C: Math. and Phys. Sci* Vol 34., 163-187

STREHLOW, R. A., LIAUGMINAS, R. WATSON, R. H. & EYMAN, J. R. 1967 Transverse wave structures in detonation, *Eleventh Symposium (International) on Combustion.* pp. 683-691. Pittsburgh: The Combustion Institute.

WOOD, W. W. AND KIRKWOOD, J. G. 1954 Diameter effects in condensed explosives: The relation between velocity and radius of curvature. *Journal of Chemical Physics*, 22: 1920-1924.

YAO, JIN AND STEWART, D. S. 1994 On the normal detonation shock velocity curvature relationship for materials with large- activation energy. *Combustion and Flame*, to appear

YAO, JIN 1995 PhD. thesis, Theoretical and Applied Mechanics University of Illinois

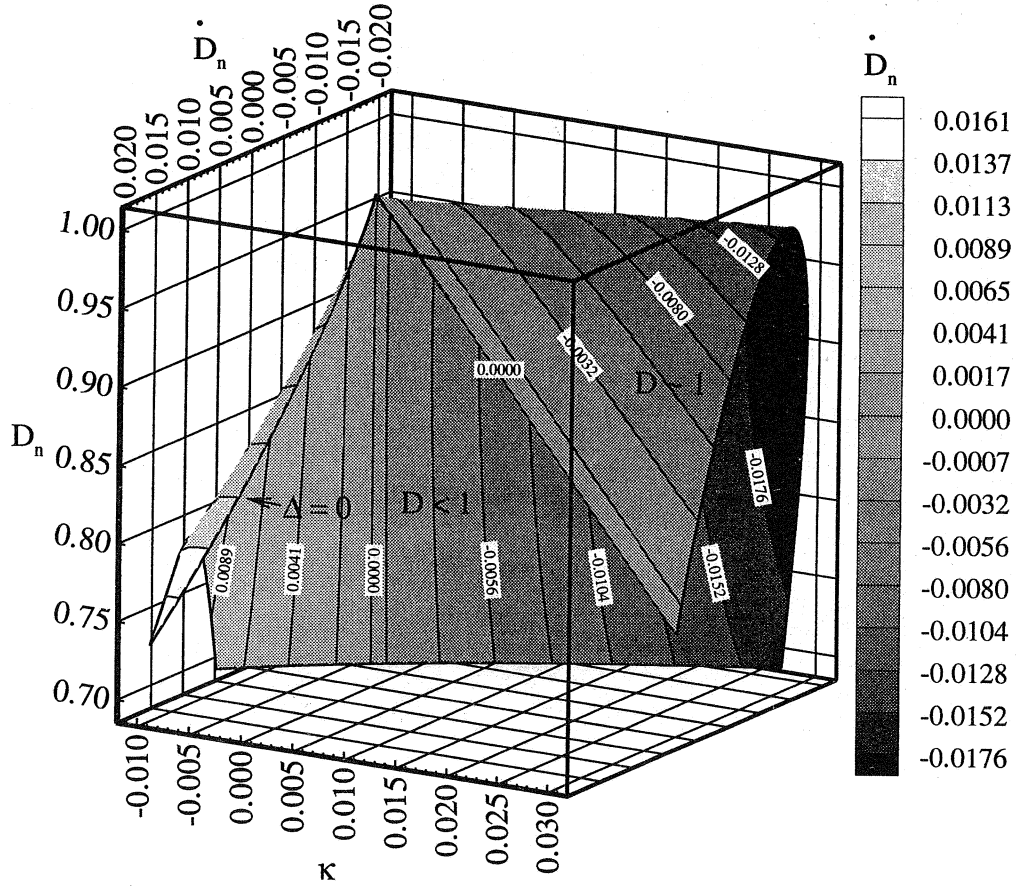

FIGURE 1 (a). Surface plot of the $\dot{D}_n - D_n - \kappa$-relation for the condensed-phase case, with $\gamma = 3, \nu = 1/2$. The curvature κ, is scaled with respect to the 1/2- reaction length. Contours of constant $\dot{D}_n$ are shown and labeled.

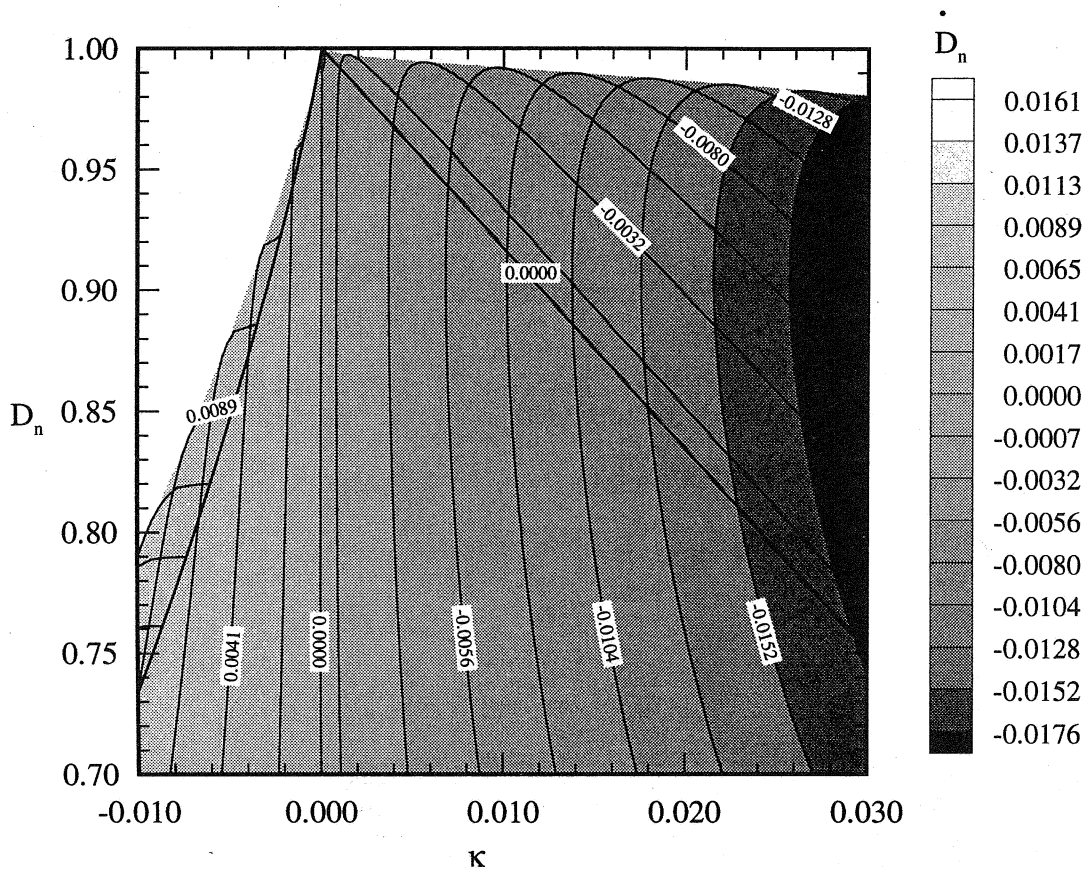

FIGURE 1 (b). Projection of the $\dot{D}_n - D_n - \kappa$-relation to the $D_n - \kappa$ -plane, for the condensed-phase case. The branch $D \sim 1$ is transparent, and the branch $D < 1$ is shown in gray-scale. Contours of $\dot{D}_n$ are indicated by the labels.

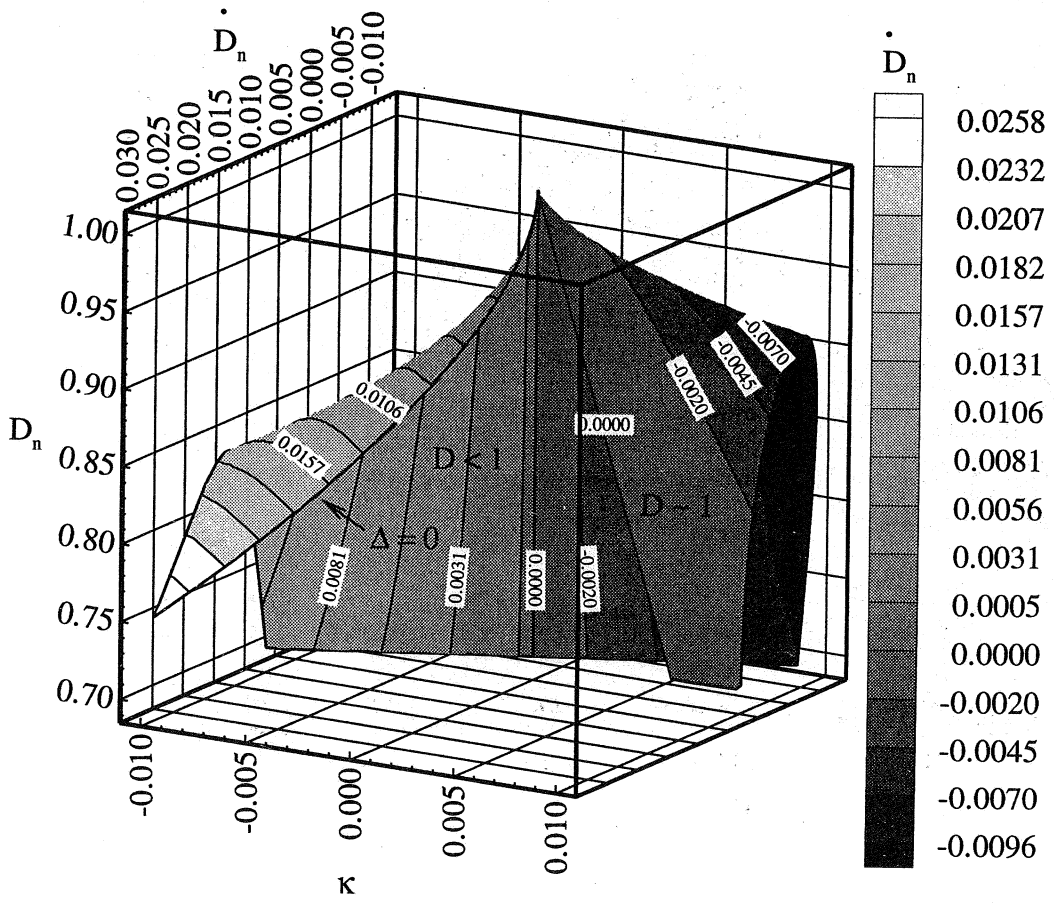

FIGURE 2 (a).Surface plot of the $\dot{D}_n - D_n - \kappa$-relation for the gas-phase case, with $\gamma = 1.2, \nu = 1$, with zero activation-energy. The curvature κ, is scaled with respect to the 1/2- reaction length. Contours of constant $\dot{D}_n$ are shown and labeled.

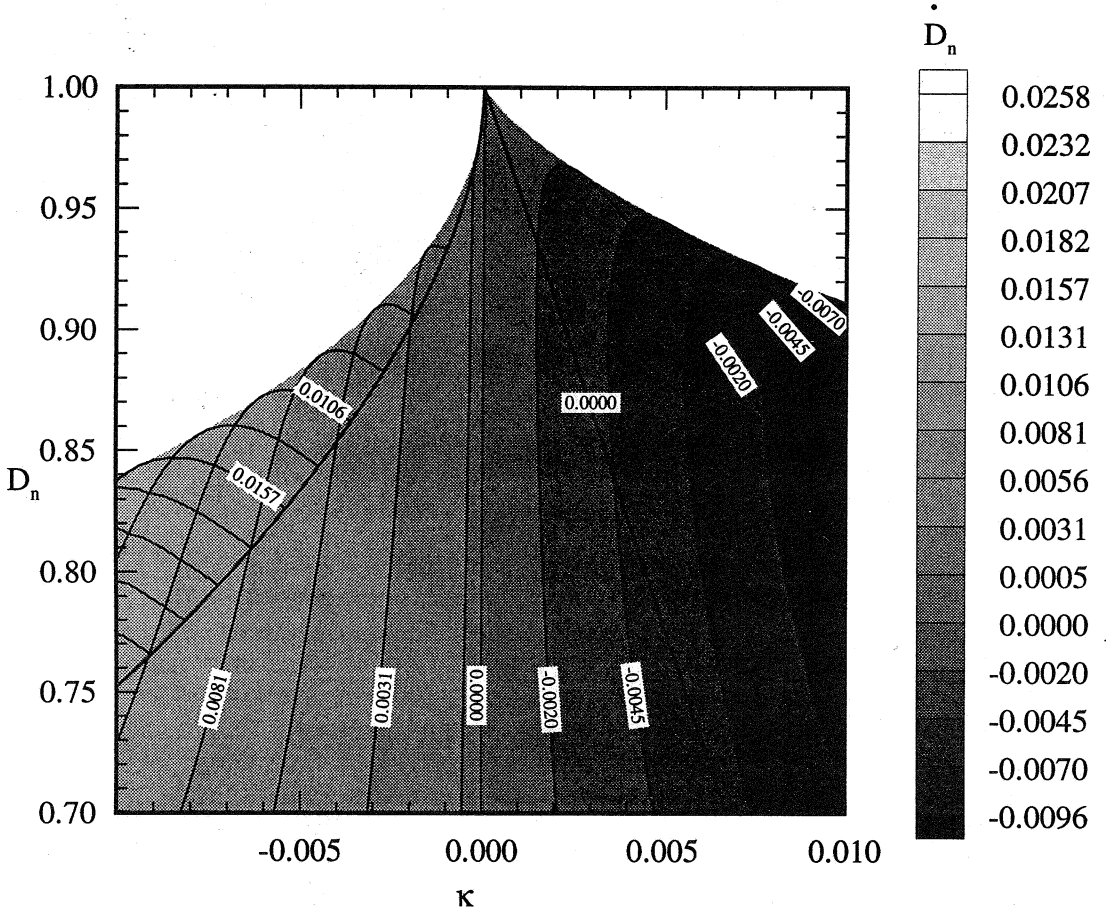

FIGURE 2 (b). Projection of the $\dot{D}_n - D_n - \kappa$-relation to the $D_n - \kappa$ -plane, for the gas-phase case, with zero activation-energy. The branch $D \sim 1$ is transparent, and the branch $D < 1$ is shown in gray-scale. Contours of $\dot{D}_n$ are indicated by the labels.

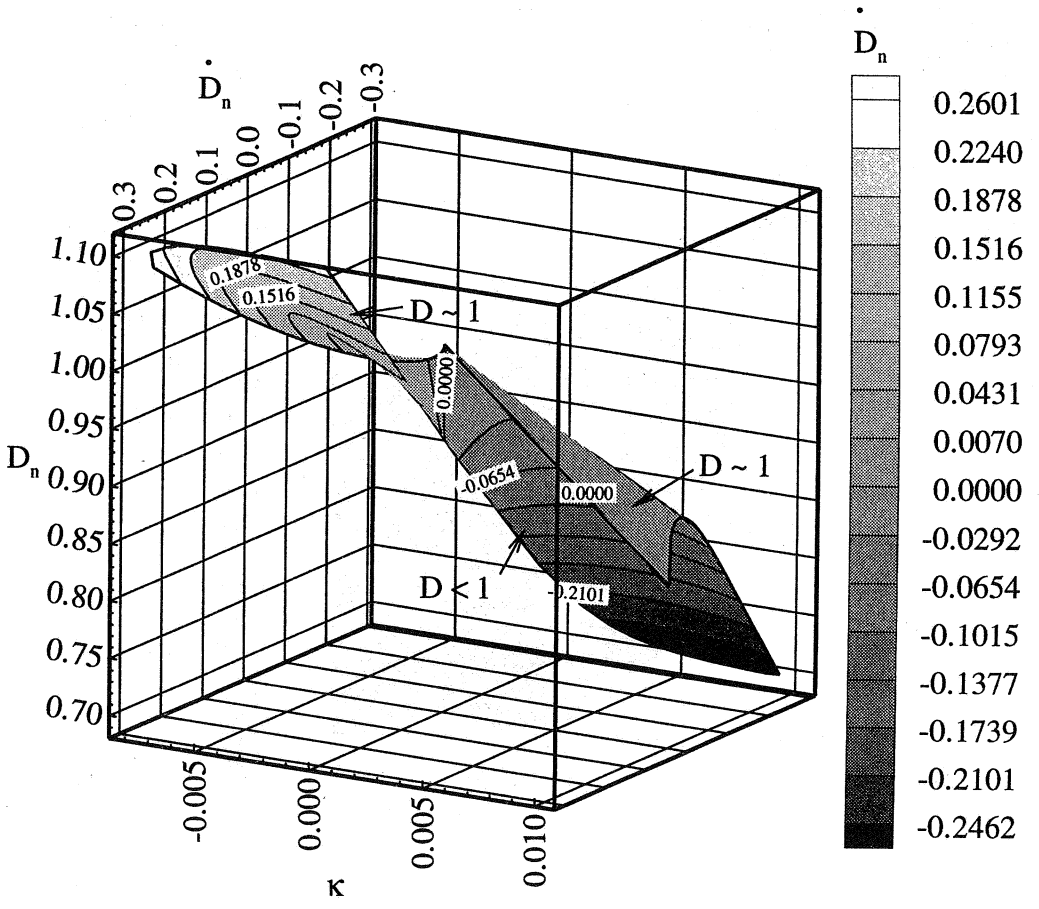

FIGURE 3 (a). Surface plot of the $\dot{D}_n - D_n - \kappa$-relation for the gas-phase case, with $\gamma = 1.2, \nu = 1$, and activation-energy, $\theta = 4/11$, $(E = 16)$, The curvature κ, is scaled with respect to the 1/2- reaction length. Contours of constant $\dot{D}_n$ are shown and labeled.

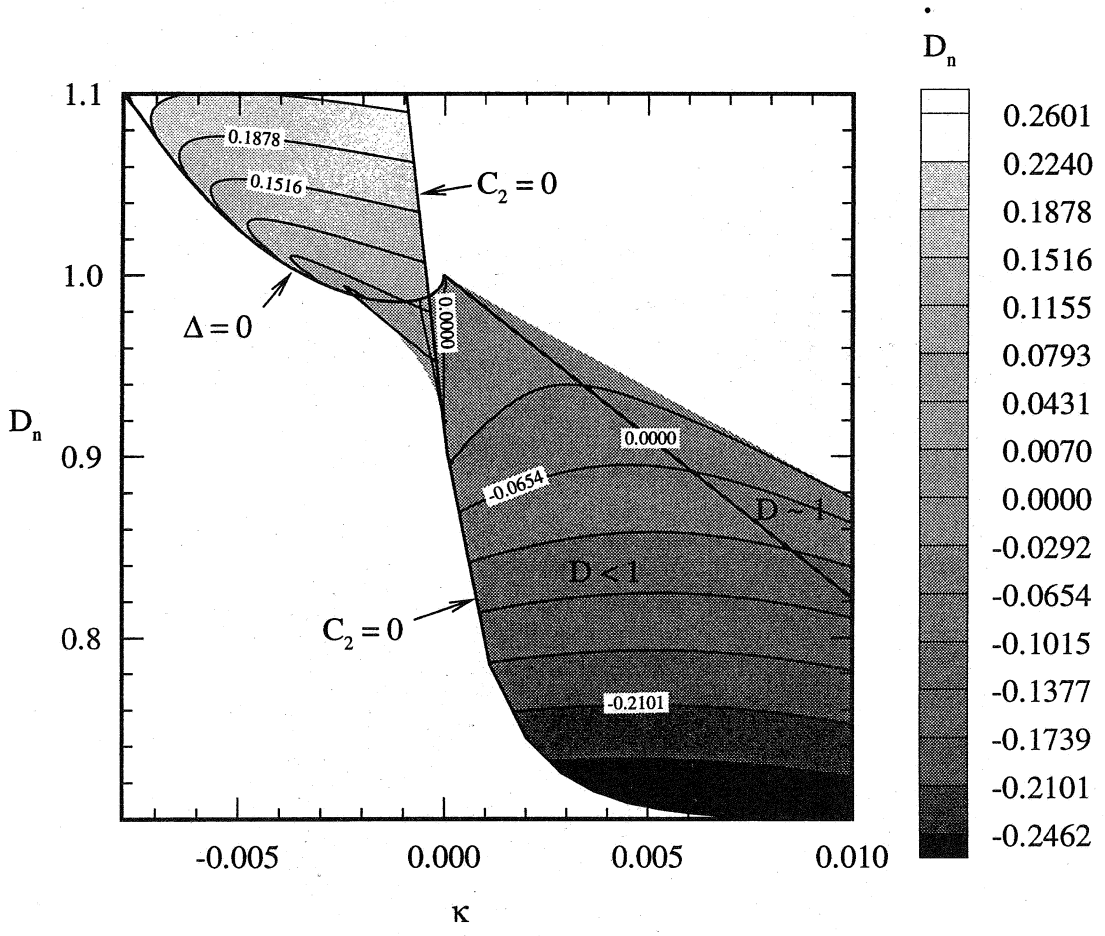

FIGURE 3 (b).Projection of the $\dot{D}_n - D_n - \kappa$-relation for the gas-phase case, with $\gamma = 1.2, \nu = 1$, and activation-energy, $\theta = 4/11$, $(E = 16)$. The branch $D \sim 1$ is transparent, and the branch $D < 1$ is shown in gray-scale. Contours of $\dot{D}_n$ are indicated by the labels.

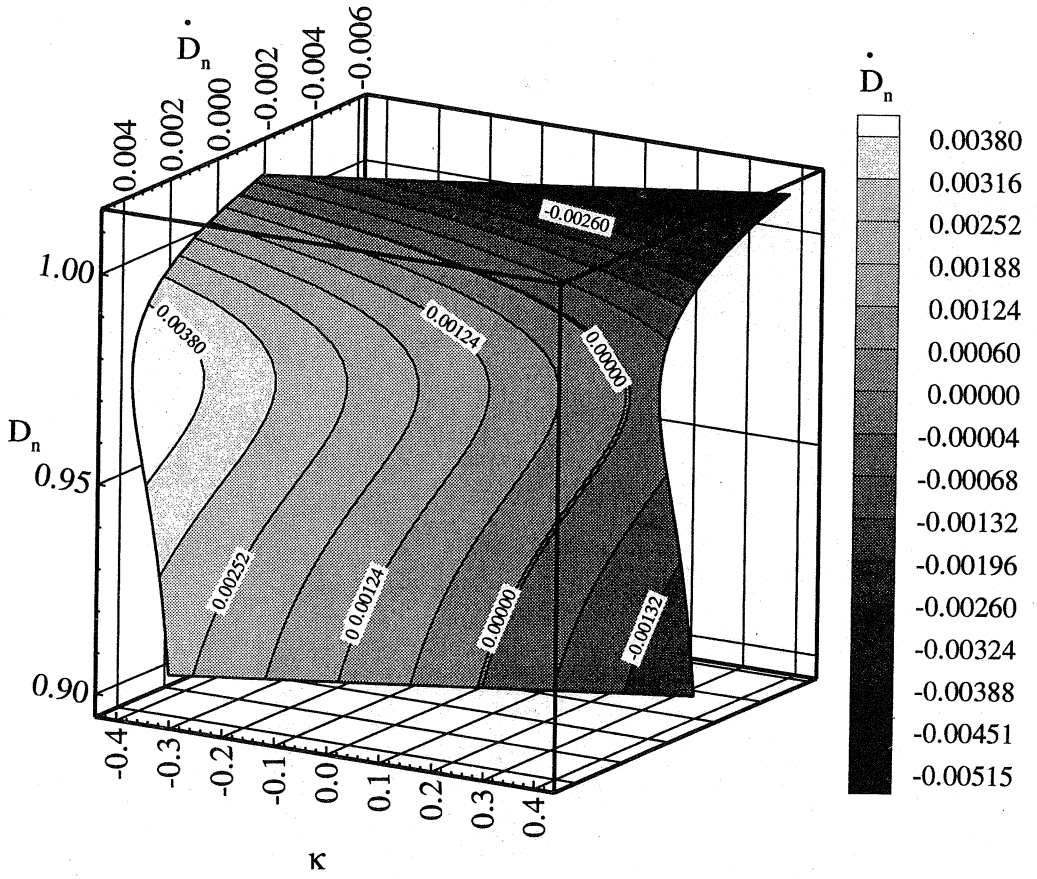

FIGURE 4 (a). Surface plot of the $\dot{D}_n - D_n - \kappa$-relation for the large-activation-energy distinguished limit discussed in section 6., with $\gamma = 1.2, \theta = 3$. The curvature κ, is scaled with respect to the induction-zone length reaction length. Contours of constant $\dot{D}_n$ are shown and labeled.

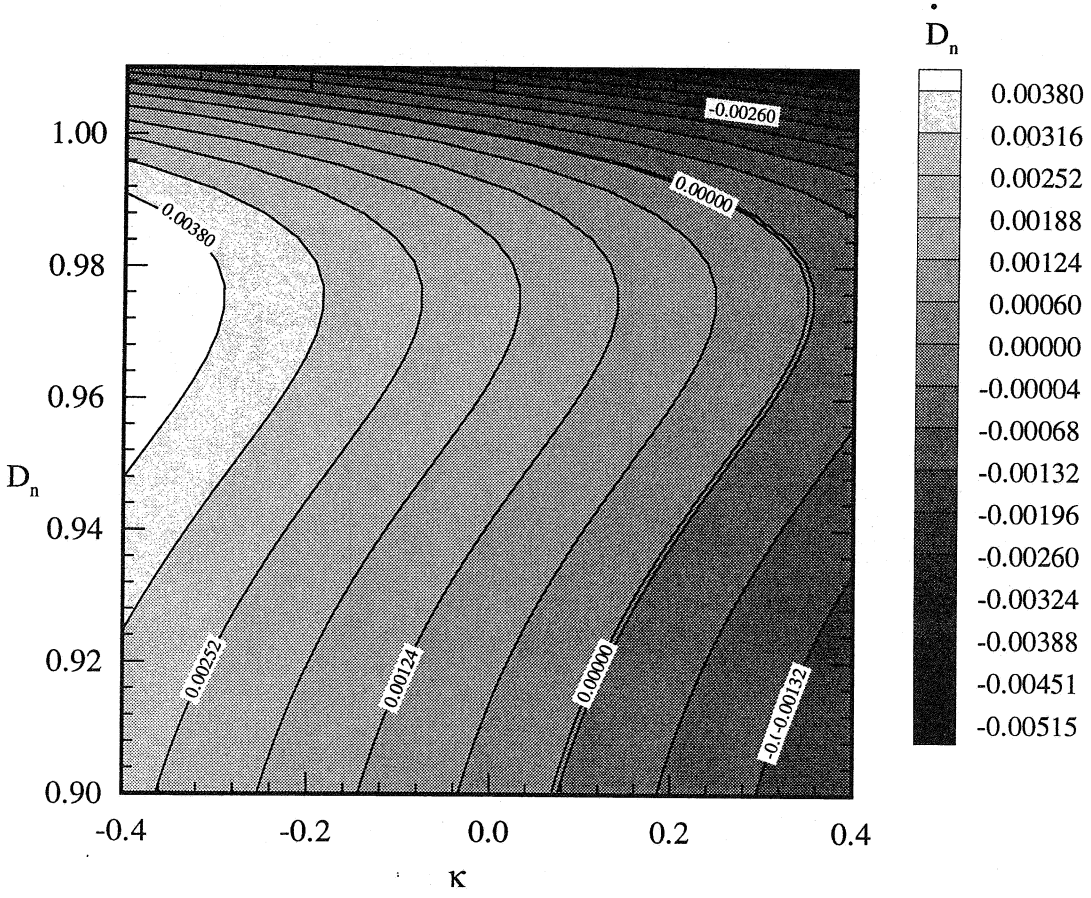

FIGURE 4 (b).Projection of the $\dot{D}_n - D_n - \kappa$-relation to the $D_n - \kappa$ -plane, for the large activation-energy distinguished limit discussed in section 6., with $\gamma = 1.2, \theta = 3$. Contours of $\dot{D}_n$ are indicated by the labels.

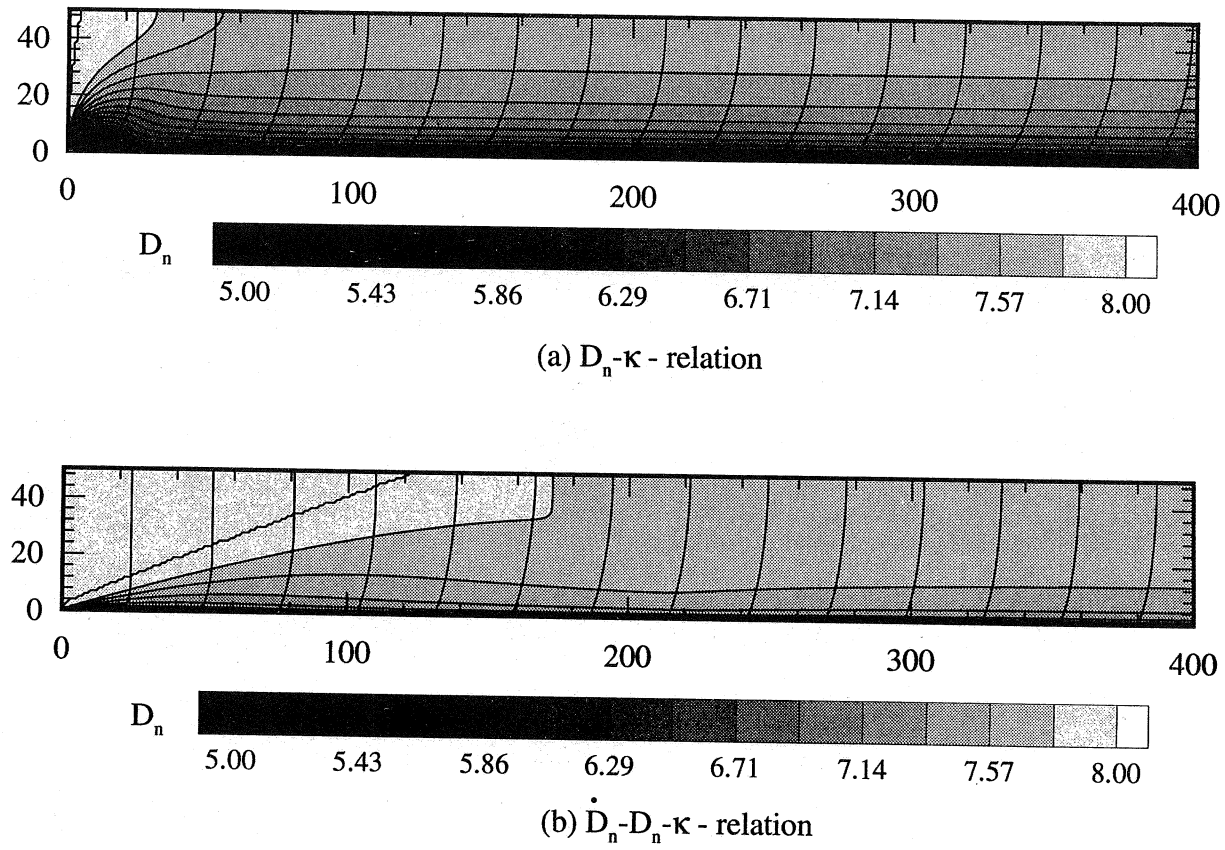

FIGURE 5. The top figure (a), corresponds to the solution of the $D_n - \kappa$ - relation of equation (7.2). The bottom figure (b) corresponds to a solution of the $\dot{D}_n - D_n - \kappa$-relation given by (7.1). The gray-scale records values of D_n at a fixed point when the shock crosses it. The first shock position from the left is at $3\,\mu$ sec, and the time intervals between subsequent shocks is 3.61μ sec.

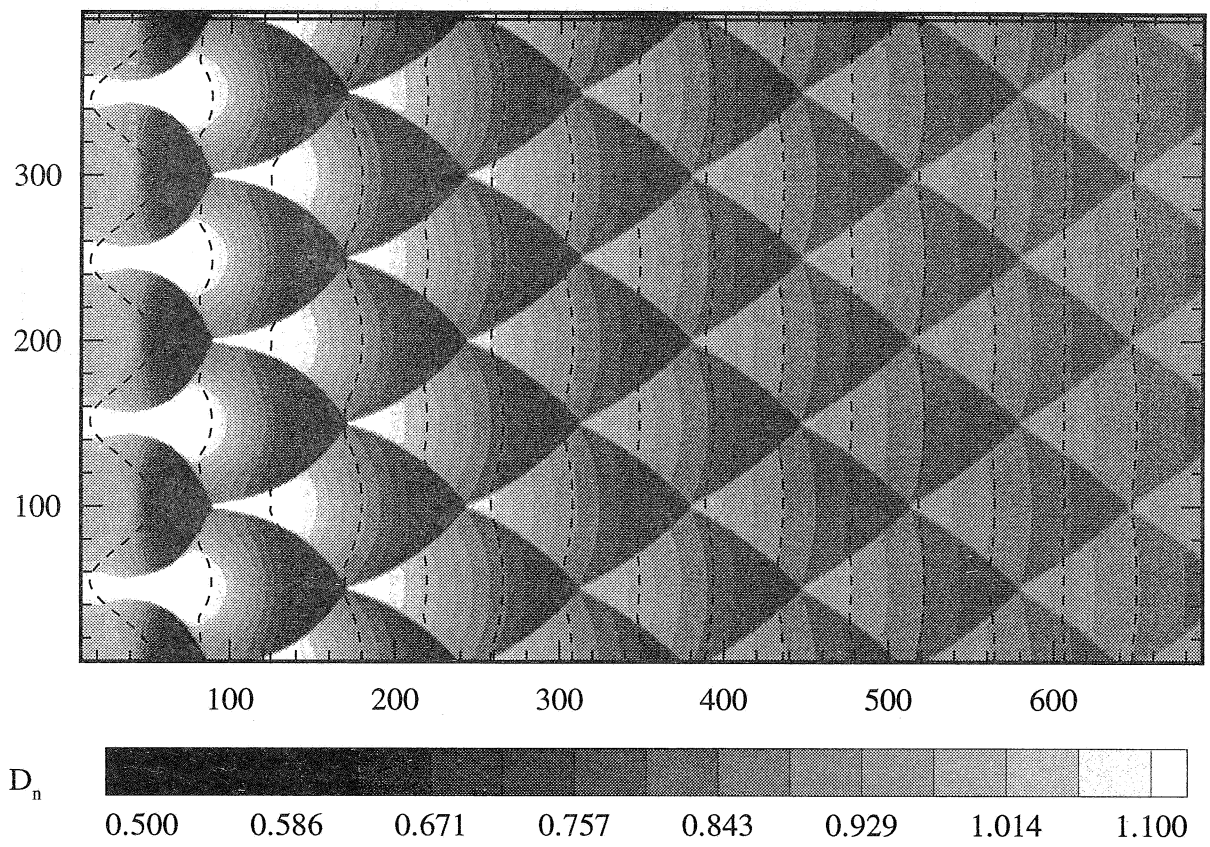

FIGURE 6. Corresponds to the numerical solution of the $\dot{D}_n - \kappa$-relation given by (7.3). The gray-scale records values of D_n at a fixed point when the shock crosses it. The shock position is show by the broken line, and is spaced at equal time intervals. The boundaries that define the patterns correspond to discontinuous jumps in the value of D_n across portions of the shock.

List of Recent TAM Reports

No.	Authors	Title	Date
731	Acharya, A., and T. G. Shawki	A second-deformation-gradient theory of plasticity	Oct. 1993
732	Michaleris, P., D. A. Tortorelli, and C. A. Vidal	Tangent operators and design sensitivity formulations for transient nonlinear coupled problems with applications to elasto-plasticity	Nov. 1993
733	Michaleris, P., D. A. Tortorelli, and C. A. Vidal	Analysis and optimization of weakly coupled thermo-elasto-plastic systems with applications to weldment design	Nov. 1993
734	Ford, D. K., and D. S. Stewart	Probabilistic modeling of propellant beds exposed to strong stimulus	Nov. 1993
735	Mei, R., R. J. Adrian, and T. J. Hanratty	Particle dispersion in isotropic turbulence under the influence of non-Stokesian drag and gravitational settling	Nov. 1993
736	Dey, N., D. F. Socie, and K. J. Hsia	Static and cyclic fatigue failure at high temperature in ceramics containing grain boundary viscous phase: Part I—Experiments	Nov. 1993
737	Dey, N., D. F. Socie, and K. J. Hsia	Static and cyclic fatigue failure at high temperature in ceramics containing grain boundary viscous phase: Part II—Modelling	Nov. 1993
738	Turner, J. A., and R. L. Weaver	Radiative transfer and multiple scattering of diffuse ultrasound in polycrystalline media	Nov. 1993
739	Qi, Q., and R. E. Johnson	Resin flows through a porous fiber collection in pultrusion processing	Dec. 1993
740	Weaver, R. L., W. Sachse, and K. Y. Kim	Transient elastic waves in a transversely isotropic plate	Dec. 1993
741	Zhang, Y., and R. L. Weaver	Scattering from a thin random fluid layer	Dec. 1993
742	Weaver, R. L., and W. Sachse	Diffusion of ultrasound in a glass bead slurry	Dec. 1993
743	Sundermeyer, J. N., and R. L. Weaver	On crack identification and characterization in a beam by nonlinear vibration analysis	Dec. 1993
744	Li, L., and N. R. Sottos	Predictions of static displacements in 1–3 piezocomposites	Dec. 1993
745	Jones, S. W.	Chaotic advection and dispersion	Jan. 1994
746	Stewart, D. S., and J. Yao	Critical detonation shock curvature and failure dynamics: Developments in the theory of detonation shock dynamics	Feb. 1994
747	Mei, R., and R. J. Adrian	Effect of Reynolds-number-dependent turbulence structure on the dispersion of fluid and particles	Feb. 1994
748	Liu, Z.-C., R. J. Adrian, and T. J. Hanratty	Reynolds-number similarity of orthogonal decomposition of the outer layer of turbulent wall flow	Feb. 1994
749	Barnhart, D. H., R. J. Adrian, and G. C. Papen	Phase-conjugate holographic system for high-resolution particle image velocimetry	Feb. 1994
750	Qi, Q., W. D. O'Brien Jr., and J. G. Harris	The propagation of ultrasonic waves through a bubbly liquid into tissue: A linear analysis	Mar. 1994
751	Mittal, R., and S. Balachandar	Direct numerical simulation of flow past elliptic cylinders	May 1994
752	Anderson, D. N., J. R. Dahlen, M. J. Danyluk, A. M. Dreyer, K. M. Durkin, J. J. Kriegsmann, J. T. McGonigle, and V. Tyagi	Thirty-first student symposium on engineering mechanics, J. W. Phillips, coord.	May 1994
753	Thoroddsen, S. T.	The failure of the Kolmogorov refined similarity hypothesis in fluid turbulence	May 1994
754	Turner, J. A., and R. L. Weaver	Time dependence of multiply scattered diffuse ultrasound in polycrystalline media	June 1994
755	Riahi, D. N.	Finite-amplitude thermal convection with spatially modulated boundary temperatures	June 1994

(continued on next page)

List of Recent TAM Reports (cont'd)

No.	*Authors*	*Title*	*Date*
756	Riahi, D. N.	Renormalization group analysis for stratified turbulence	June 1994
757	Riahi, D. N.	Wave-packet convection in a porous layer with boundary imperfections	June 1994
758	Jog, C. S., and R. B. Haber	Stability of finite element models for distributed-parameter optimization and topology design	July 1994
759	Qi, Q., and G. J. Brereton	Mechanisms of removal of micron-sized particles by high-frequency ultrasonic waves	July 1994
760	Shawki, T. G.	On shear flow localization with traction-controlled boundaries	July 1994
761	Balachandar, S., D. A. Yuen, and D. M. Reuteler	High Rayleigh number convection at infinite Prandtl number with temperature-dependent viscosity	July 1994
762	Phillips, J. W.	Arthur Newell Talbot—Proceedings of a conference to honor TAM's first department head and his family	Aug. 1994
763	Man., C. S., and D. E. Carlson	On the traction problem of dead loading in linear elasticity with initial stress	Aug. 1994
764	Zhang, Y., and R. L. Weaver	Leaky Rayleigh wave scattering from elastic media with random microstructures	Aug. 1994
765	Cortese, T. A., and S. Balachandar	High-performance spectral simulation of turbulent flows in massively parallel machines with distributed memory	Aug. 1994
766	Balachandar, S.	Signature of the transition zone in the tomographic results extracted through the eigenfunctions of the two-point correlation	Sept. 1994
767	Piomelli, U.	Large-eddy simulation of turbulent flows	Sept. 1994
768	Harris, J. G., D. A. Rebinsky, and G. R. Wickham	An integrated model of scattering from an imperfect interface	Sept. 1994
769	Hsia, K. J., and Z. Xu	The mathematical framework and an approximate solution of surface crack propagation under hydraulic pressure loading	Sept. 1994
770	Balachandar, S.	Two-point correlation and its eigen-decomposition for optimal characterization of mantle convection	Oct. 1994
771	Lufrano, J. M., and P. Sofronis	Numerical analysis of the interaction of solute hydrogen atoms with the stress field of a crack	Oct. 1994
772	Aref, H., and S. W. Jones	Motion of a solid body through ideal fluid	Oct. 1994
773	Stewart, D. S., T. Aslam, J. Yao, and J. B. Bdzil	Level-set techniques applied to unsteady detonation propagation	Oct. 1994
774	Mittal, R., and S. Balachandar	Effect of three-dimensionality on the lift and drag of circular and elliptic cylinders	Oct. 1994
775	Stewart, D. S., T. D. Aslam, and Jin Yao	The evolution of detonation cells	Nov. 1994
776	Aref, H.	On the equilibrium and stability of a row of point vortices	Nov. 1994
777	Cherukuri, H. P., T. G. Shawki, and M. El-Raheb	An accurate finite-difference scheme for elastic wave propagation in a circular disk	Nov. 1994
778	Li, L., and N. R. Sottos	Improving hydrostatic performance of 1–3 piezocomposites	Dec. 1994
779	Phillips, J. W., D. L. de Camara, M. D. Lockwood, and W. C. C. Grebner	Strength of silicone breast implants	Jan. 1995
780	Xin, Y.-B., K. J. Hsia, and D. A. Lange	Quantitative characterization of the fracture surface of silicon single crystals by confocal microscopy	Jan. 1995
781	Yao, J., and D. S. Stewart	On the dynamics of multi-dimensional detonation	Jan. 1995